Résumé de la thèse – Thesis summary

Pour obtenir le grade de

DOCTEUR DE L'UNIVERSITÉ GRENOBLE ALPES
et BRNO UNIVERSITY OF TECHNOLOGY

École doctorale: PHYS - Physique
Spécialité: Physique des matériaux
Unité de recherche: Institut Néel

Réseaux artificiels de nanostructures magnétiques

Artificial arrays of magnetic nanostructures

Présentée par:

Vojtěch SCHÁNILEC

Direction de thèse:

Nicolas ROUGEMAILLE
DIRECTEUR DE RECHERCHE, CNRS – Institut Néel — Directeur de thèse

Tomáš ŠIKOLA
DIRECTEUR DE RECHERCHE,
CEITEC – Brno University of Technology — Co-Directeur de thèse

Rapporteurs:

Julian CARREY
PROFESSEUR, INSA Toulouse

Alexandra MOUGIN
DIRECTEUR DE RECHERCHE, CNRS - Université Paris-Saclay

Thèse soutenue publiquement le **12 mai 2023**, devant le jury composé de:

Julian CARREY
PROFESSEUR, INSA Toulouse — Rapporteur

Alexandra MOUGIN
DIRECTEUR DE RECHERCHE, CNRS – Université Paris-Saclay — Rapportrice

Jon Ander ARREGI URIBEETXEBARRIA
DOCTEUR EN SCIENCES, CEITEC – Brno University of Technology — Examinateur

Aleš HRABEC
DOCTEUR EN SCIENCES, ETH – Paul Scherrer Institut — Examinateur

Daniel LACOUR
DIRECTEUR DE RECHERCHE, CNRS – Institut Jean Lamour — Examinateur

Elsa LHOTEL
DIRECTEUR DE RECHERCHE, CNRS – Institut Néel — Examinatrice

Laurent RANNO
MAITRE DE CONFERENCES, Université Grenoble Alpes — Examinateur

Radimír VRBA
PROFESSEUR, CEITEC – Brno University of Technology — Examinateur

BRNO UNIVERSITY OF TECHNOLOGY

VYSOKÉ UČENÍ TECHNICKÉ V BRNĚ

CENTRAL EUROPEAN INSTITUTE OF TECHNOLOGY BUT

STŘEDOEVROPSKÝ TECHNOLOGICKÝ INSTITUT VUT

ARTIFICIALARRAYS OF MAGNETIC NANOSTRUCTURES

UMĚLÉ USPOŘÁDANÉ SOUBORY MAGNETICKÝCH NANOSTRUKTUR

DOCTORAL THESIS SUMMARY

TEZE

AUTHOR AUTOR PRÁCE	Ing. Vojtěch Schánilec
SUPERVISOR ŠKOLITEL	prof. RNDr. Tomáš Šikola, CSc.
SUPERVISOR ŠKOLITEL	Dr. Nicolas Rougemaille

BRNO 2023

Abstract

Two-dimensional artificial arrays of interacting nanomagnets are a powerful playground for probing the physics of the lattice spin models. Artificially designed spin systems were introduced to mimic the behaviour of the frustrated pyrochlore crystals. Recent improvement in nano-fabrication techniques allows us to fabricate any desired artificial system in the lab control environment. Therefore artificial simulators of the matter can be produced and used for more advanced study of the desired phenomenons.

The advantage of using nanomagnetic objects as building blocks of artificial lattices is that small magnetic structures can effectively be considered giant classical Ising spins. Therefore elevating the problem of frustrated spins in pyrochlore crystals into such dimensions so the system can be studied with real space imaging techniques.

With imaging techniques such as magnetic force microscopy, the ordering of each Ising macrospin can be visualised in real space, enabling us to look not only at the global property of the system as a whole but to see how local interactions are accommodated.

Being able to fabricate artificial systems capturing the desired physics and comparing it to the real nature counterpart measures our understanding of the problem. It can also offer a missing piece of information. Furthermore, there are properties of the systems which are emergent and not encoded in the theoretical Hamiltonians describing the systems. Such properties seem to come out of nowhere, and with artificial systems and the ability to visualise these systems, we can analyse such properties.

This thesis focus on studying two types of systems: kagome and square dipolar spin systems. Both these systems are the results of the projections of the three-dimensional pyrochlore crystals into a plane. Moreover, both systems exhibit rather unusual behaviour, which is still to be measured on a large scale in real space. The dipolar kagome spin system has a low energy phase called *spin liquid 2*, which hosts unusual spin behaviour. The spins in this phase are ordered and disordered simultaneously, a unique emergent property of the system with no equivalent.

On the other hand, the square spin system is a perfect playground for studying the exotic physics of spin liquids, the Columb phase, and the behaviour of magnetic monopole-like quasi-particles.

The usual approach when fabricating artificial spin systems is to build them up out of single-domain nanomagnets which interact via long-range dipolar interactions. Therefore the systems try to minimise the interactions between all pairs of the Ising macrospins. However, the central idea of this thesis is to connect all the nanomagnets into one macro lattice, therefore introducing the micromagnetic effects into the systems. Magnetisation tries to satisfy the micromagnetic energies at the vertex site. Hence, we effectively replace the spin degree of freedom with a micromagnetic knob which can be used to tune each vertex's energy by introducing specially designed topological defects.

Even though both systems have been the focus of researchers for almost twenty years, we believe that our modifications open a gateway to fully accessing the exotic physic yet to uncover.

Abstrakt

Uměle vytvořená dvourozměrná pole interagujících nanomagnetů jsou mocným hřištěm pro zkoumání fyziky mřížkových spinových modelů. Tyto umělé spinové systémy byly navrženy tak, aby napodobovaly chování frustrovaných pyrochlorových krystalů. Zdokonalení nanofabrikačních technik nám umožňuje vyrobit jakýkoli požadovaný umělý systém v laboratorně kontrolovaném prostředí. Díky tomu lze vyrábět umělé simulátory hmoty a používat je k pokročilejšímu studiu požadovaných jevů.

Výhodou použití nanomagnetických objektů jako stavebních kamenů umělých mřížek je, že malé magnetické struktury lze efektivně považovat za obří klasické Isingovy spiny. Proto transformují problém frustrovaných spinů v pyrochlorových krystalech do takových rozměrů, aby bylo možné systém studovat pomocí zobrazovacích technik reálného prostoru.

Pomocí zobrazovacích technik, jako je mikroskopie magnetických sil, lze uspořádání každého Isingova makrospinu vizualizovat v reálném prostoru. To nám umožní podívat se nejen na globální vlastnost systému jako celku, ale také na to, jak jsou realizovány lokální interakce.

Schopnost vyrobit umělé systémy zachycující požadovaný fyzikální jev a porovnat jej s reálným přírodním protějškem ukazuje naše porozumění problému. Může také nabídnout chybějící část informací. Existují vlastnosti systémů, které nejsou zakódovány v teoretických Hamiltoniánech popisujících systémy, ale přesto jsou systému vlastní. Takové vlastnosti se zdánlivě objevují odnikud a díky umělým systémům a schopnosti tyto systémy vizualizovat můžeme takové vlastnosti analyzovat.

Tato práce se zaměřuje na studium dvou typů systémů: kagome a čtvercových dipolárních spinových systémů. Oba tyto systémy jsou výsledkem projekcí trojrozměrných pyrochlorových krystalů do roviny. Oba navíc vykazují poměrně neobvyklé chování, které je třeba teprve změřit v reálném prostoru ve velkých měřítcích. Dipolární kagome spinový systém má nízkoenergetickou fázi zvanou *spinová kapalina 2*. Spiny v této fázi jsou uspořádané a neuspořádané současně, což je jedinečná vlastnost systému, která nemá obdoby. Na druhé straně, čtvercový spinový systém je dokonalým hřištěm pro studium exotické fyziky spinových kapalin, Columbovy fáze a chování kvazičástic podobných magnetickým monopólům.

Obvyklý přístup při výrobě umělých spinových systémů spočívá v jejich sestavení z jednodoménových nanomagnetů, které interagují prostřednictvím dipolárních interakcí dlouhého dosahu. Systémy se proto snaží minimalizovat interakce mezi všemi páry Isingových makro-spinů. Ústřední myšlenkou této práce je však propojení všech nanomagnetů do jedné makromřížky, a tedy zavedení mikromagnetických efektů do systémů. Magnetizace se snaží uspokojit mikromagnetické energie v místě spojů. Proto účinně nahrazujeme spinový stupeň volnosti mikromagnetickým regulátorem, který lze použít k vyladění energie každého spoje zavedením speciálně navržených topologických defektů.

Přestože oba systémy jsou předmětem zájmu výzkumníků již téměř dvacet let, věříme, že naše modifikace otevírají bránu ke zkoumání exotické fyziky, kterou je třeba teprve odhalit.

Key words

Artificial spin systems, geometrical frustration, micromagnetism, kagome dipolar spin system, square spin system

Klíčová slova

Umělé vytvořené spinové systémy, geometrická frustrace, mikromagnetismus, dipolární kagome spinový systém, čtvercový spinový systém

Contents

Chapter 1: Introduction

The main goal of this thesis is to provide a new point of view on artificial spin systems and how currently used design can be improved by implementing the micromagnetic effects.

This summary presents only the introduction to artificial spin ice systems and the motivation for our work. The thesis has an extra section containing the selected basics of micromagnetism, the principle of geometrical frustration, and the origin of artificial spin ice systems and their evolution.

1.1. Artificial spin ice

Two-dimensional artificially fabricated systems capturing the physics of frustrated spin ice (pyrochlore) crystals are called *artificial spin ice systems*.

At the beginning of the millennium, Tanaka et al. [1,2], and Wang et al. [3] successfully fabricated artificial arrays of nanomagnets that captured some behaviour of the frustrated spin ice systems, but in the two-dimension lattices. With the improvements in nanofabrication techniques, the design of artificial systems can get more complex and better at capturing the physic that would be difficult or impossible to observe in nature. There are two possibilities for how the 3D spin ice geometry can be transferred into 2D geometry.

The artificial kagome geometry

Figure 1.1 a) shows an example of how the artificial kagome lattice can look. There are more ways the lattice can be realised, and they are discussed more in Chapter 3 of the thesis.

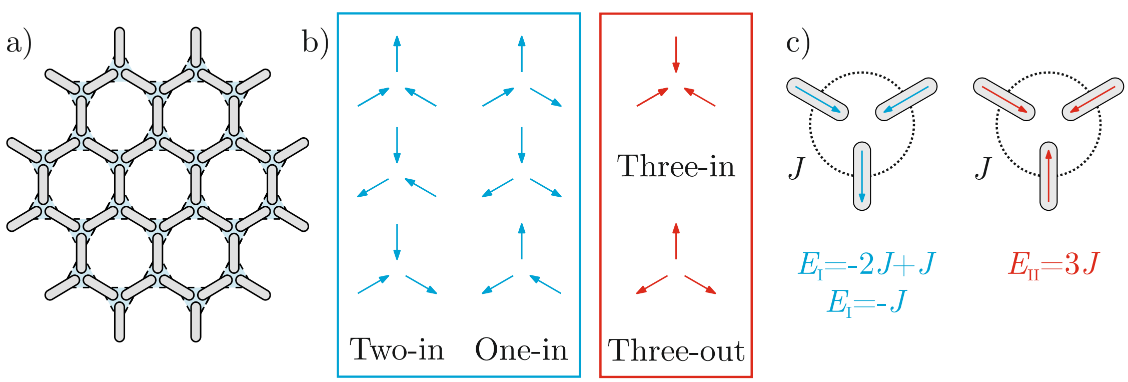

Figure 1.1: a) Artificial kagome spin ice lattice, grey nanomagnets are placed on the apex of the kagome layout (blue triangles), forming the lattice. b) Six possible ground state configurations obey the kagome ice-rules (blue frame) and two ice-rules breaking high-energy configuration (red frame). The ground state energies and high-energy configurations are shown in c), where J is the coupling strength constant between the spins.

The vertices are geometrically frustrated since the "macrospins" (single domain nanomagnets) interact via dipolar interaction. They minimise their interaction if they point head to tail, which is impossible for all three pairs of spins in the vertex. The ground state spin configuration follows the kagome modified ice-rule: two-spin outside or two-spin inside of the vertex, and it is six times degenerated as is shown in Figure 1.1 b) in the blue frame. In terms of the J coupling strength constant, the energy of the ground state configuration is $E_{\mathrm{I}} = -2J + J = -J$ since two interactions are minimise ($-2J$), and one is maximised (J). The other two high-energy spin configurations have no interaction minimised, and the total energy of these vertexes is $E_{\mathrm{II}} = 3J$. The J coupling constant's strength can be tuned by changing the spacing between the nanomagnets.

This type of kagome realisation can be called an artificial spin ice system. Since the ground state is six times degenerated, and the geometry is derived from the ice and spin ice systems, even though there are sixteen possible vertex types in ice or spin ice systems.

The artificial square geometry

The pioneering work on the artificial square geometry was done by Wang et al. [3]. Wang introduced the square spin geometry shown in Figure 1.2 a). The lattice is made of single-domain Ising-like nanomagnets placed on a layout made of edge projection of pyrochlore crystal (the blue square layout).

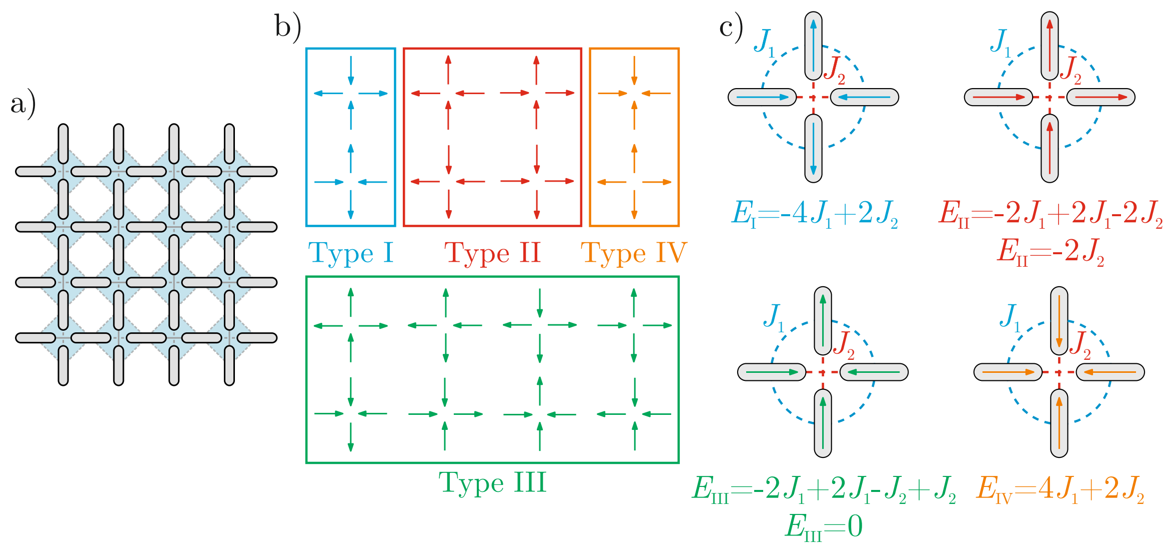

Figure 1.2: a) Wang's square lattice, nanomagnets (grey islands) are put at the apex of square ice projections (blue squares). Sixteen possible spin configurations in square vertex. Type I and II are ice-rules obeying configurations. Type III and IV are high-energy ice-rule-breaking configurations. The total energy of each type of configuration is calculated in c), where J_1 is the coupling constant between the first nearest neighbours a J_2 between the seconds.

There are sixteen possible spin configurations (divided into four types), since each vertex has four spins with two possible orientations similar to the ice and spin ice systems. All possible spin configurations are shown in Figure 1.2 b). Contrary to the spin ice vertices, in the artificial square spin system, the interacting nanomagnets do not have the same interaction strength. Therefore, there needs to be considered two types of neighbours in the vertex. The first nearest neighbours are perpendicular to each other, and their coupling constant is J_1. The second neighbours are parallel and their coupling strength constant is J_2. The energy of each vertex type in the multiple of J_1 and J_2 are shown in Figure 1.2 c).

Because the transformation into a two-dimensional system breaks the system's symmetry, and because $J_1 > J_2$ the ground state spin configuration of Wang's square lattice is only two times degenerated, this system should not be called an artificial spin ice system.

One of the goals of this thesis is to design a new square lattice where the symmetry would be restored. Chapter 4 is dedicated to the description of the square geometry.

1.2. Motivation and overview of the thesis

The exotic physics of frustrated systems are usually well-known and described theoretically. However, designing an artificial system which captures the desired behaviour so it can be measured in real space is still very challenging, even with all the development in nanofabrication techniques.

The motivation for this work is twofold. We want to invent and test new designs of artificial spin systems which are better at capturing the physics of different spin and vertex models connected to spin liquid physics. We prove that the newly designed lattices are functional within the theoretical frameworks and use them to understand the theoretical models better.

The main idea behind this thesis is to change the lattices by using connected nanomagnets instead of disconnected ones. These connections transform the system from a spin system, where the physics is driven by many body dipolar interactions between individual spins, into a vertex system. In the vertex system, the physic is now driven by the micromagnetic energies at the vertex sites. We can tune the micromagnetic interactions almost at will by designing special defects at the vertex sites of the connection nanomagnets. By changing the vertex geometry, we can force the system to change its ground state configuration and configuration of excited states.

Chapter 3 presents the kagome lattice with notches as a new artificial spin system. The main problem with the kagome dipolar spin ice systems (with disconnected nanomagnets) is that it is near to impossible to force the system into low-energy spin configurations. The reasons why it is impossible are discussed in the chapter. However, our approach can bypass these limitations and prepare lattice capturing the spin configuration of low-energy phases of the kagome system.

In Chapter 4, we show how the lost degeneracy of the Wang artificial lattice can be restored. Furthermore, our approach can be practically used for researching individual realisation of possible vertex models connected to the square and ice geometry. We also provide the experiment based on our new lattice, which allowed us to observe real space infinite order phase transition in one of the F model [4], which is one of the celebrated vertex models.

Our results could be a gateway to a more precise study of a wide range of frustrated spin and vertex models.

Chapter 2: Methodology

Our experimental strategy relies heavily on designing new lattices that would better capture the physics of spin systems. We focus on two-dimensional artificial kagome and square spin systems described in the previous chapter. The key element of our research is redesigning the geometry of these systems to control the driving physics. By physically connecting the individual single-domain nanoislands into one macro lattice, we are transferring the spin system into the vertex system. At each vertex site, micromagnetic energies compete over the resulting configuration.

Therefore, central idea of this work is to replace the spin degree of freedom with a local "*micromagnetic knob*", which can be used to finely tune the total micromagnetic vertex energy.

In order to predict the behaviour of our newly design artificial spin systems, Monte Carlo and Mumax^3 simulations are conducted.

After the target properties of lattices are acquired from simulation, the lattices are fabricated by *Electron beam lithography* (EBL). The required material is deposed by *Electron beam physical vapour deposition* (EBPVD). Fabricated samples are checked by *Scanning electron microscopy* (SEM) to see the quality of the sample. The fabrication techniques are described in section 2.1.

Magnetic field demagnetisation brings the magnetic samples into their low-energy configurations.

To acquire information about the sample's magnetic configuration, *Magnetic force microscopy* (MFM) is used. From MFM outputs, the analysis is done by various in-house custom build software. MFM technique and data analysis processes are described in section 2.2. In this summary, only crucial information about the sample fabrication and data analysis are provided, for full description see the thesis.

2.1. Sample fabrication

Fabrication of all samples used during the research described in this manuscript was done with a one-step lift-off procedure. The EBL was done either with E-beam writer RAITH150 Two (RAITH) in BUT CEITEC research laboratory or Nanobeam Nb5 in Nanofab Institut Néel.

The magnetic objects forming our lattices are thermally stable, and their magnetic configuration is not affected by the temperature. As such, all measurements can be done at room temperature.

2.1.1. Electron beam lithography

The EBL is a well-known technique for fabrication in nanoscience. Due to the precision (even sub 10 nm [5, 6] resolution) that EBL can reach, it is the perfect tool for designing and fabricating lattices of interacting nanomagnets that can capture the physics of spin liquids described in the previous chapter. This technique allows us to design our lattice with precise variations in geometry, enabling us to control the role of micromagnetic interaction almost at will.

Both studied lattices have different response to imperfect fabrication. The kagome lattices with notches which vertex can be seen in Figure 2.2 a) benefits from the fact that we are deliberately breaking the system's symmetry. Both magnetostatics and magnetodynamics are entirely driven by the notch defect.

On the other hand, the second type of geometry we study is the square lattice with holes which vertex is shown in Figure 2.2 b). The addition of the "hole defect" at the vertex site is not breaking the symmetry of the system if the hole is indeed circular. Since we rely on the hole governing the physics, the fabrication needs to be done as precisely as possible.

Fabricating the square lattice with holes is more complicated than the kagome lattice with notches. However, after several optimisation procedures and dose sweep strategy, all lattices can be reproducibly fabricated, capturing the physic of spin systems described in the following chapters.

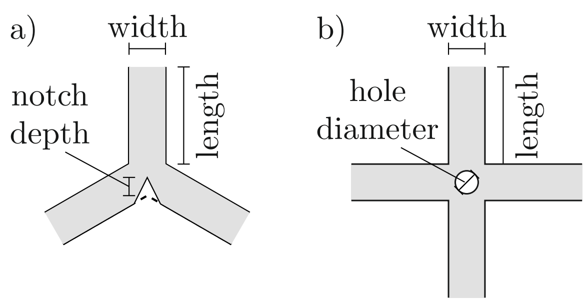

Figure 2.1: The schema of the vertices of a) kagome lattice with notches and b) square lattice with holes. The symmetry of the kagome vertex with notch is broken by design. Therefore it is less susceptible to defects caused by the fabrication process than the perfectly symmetric square vertex with hole.

Both kagome lattices with notches and square spin systems with holes presented different non-trivial challenges during the fabrication process.

In the case of kagome lattices, the fabrication was easily done after the layout designs. The main problem was finding an effective and flawless process to produce a series of layouts needed for research efficiency. Figure 2.2 a) shows an example of a fabricated aperiodic lattice.

On the other hand, square spin systems were always easy to design. They are periodic, and the hole at the vertex site is the same all over the lattice, as shown in Figure 2.2 b). However, the hole diameter changes the physics drastically even if the hole diameter changes only by a few nanometers. The sensitivity of hole diameter require perfectly done lithographic procedures.

Figure 2.3 shows a set of SEM images of lattices with holes. The width of the connected islands is 100 nm, the distance from the centre of the vertex to the vertex is 500 nm, and the thickness is 25 nm. The hole diameter is the only parameter that changes between the fabricated lattices. If the hole diameter is too small, as is in the case of the nominal value of 64 nm, the resist and the magnetic material from the centre of the vertex are not

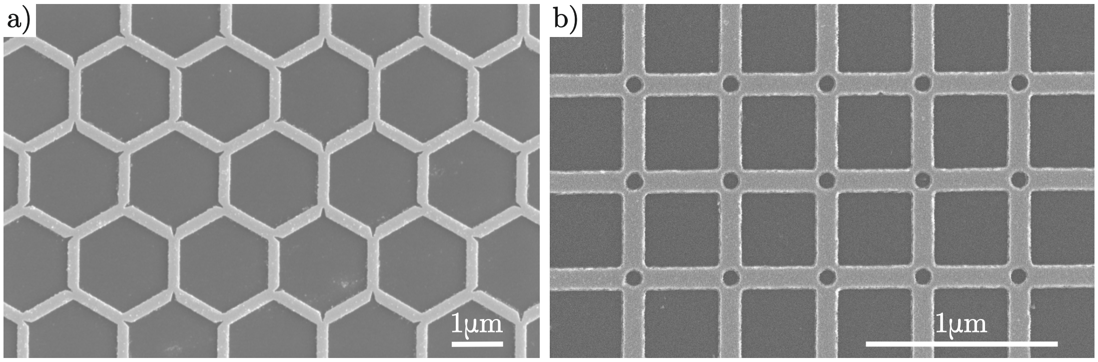

Figure 2.2: SEM images of a) kagome lattice with notch and b) square lattice with holes.

properly lifted off and collapse. We can observe the fallen pillars at some vertex sites. On the other hand, the material is not fully lifted-off at some vertex sites, and during the ultrasound bath, it breaks off with a part of the lattice. Therefore all lattices we fabricated with hole diameters 64 nm and smaller are unusable. The series of lattices we used for our research described in Chapter 4 have hole diameters from 72 nm to 120 nm.

Ing. Ondřej Brunn was involved in fabricating the square system with holes. His involvement included operation with the Nanobeam litograph Nb5 at Nanofab Institut Néel and choosing the right combination of chemicals to reach the limit of the lithographic technique.

Sample parameters

Every modified kagome lattice with notches consists of 627 vertices. Each nanoisland has an aspect ratio of 5, where the width of the nanomagnet is 200 nm, and the length is $1\,\mu$m. The thickness is 15 nm. The fabrication material is NiFe. The depth of the notch varies from $100 - 250$ nm, but is always constant in a given lattice. The lattices have a size of approximately $30 \times 30\,\mu$m.

The square system with holes consists of 900 vertices, and each nanoisland has an aspect ratio of 5. The width of the nanomagnets is 100 nm, and the length is 500 nm. The lattice is made from NiFe, and its thickness is 25 nm. The hole diameter varies from $0 - 155$ nm, but it is always constant for the given lattice. Square lattices have a size of approximately $16 \times 16\,\mu$m

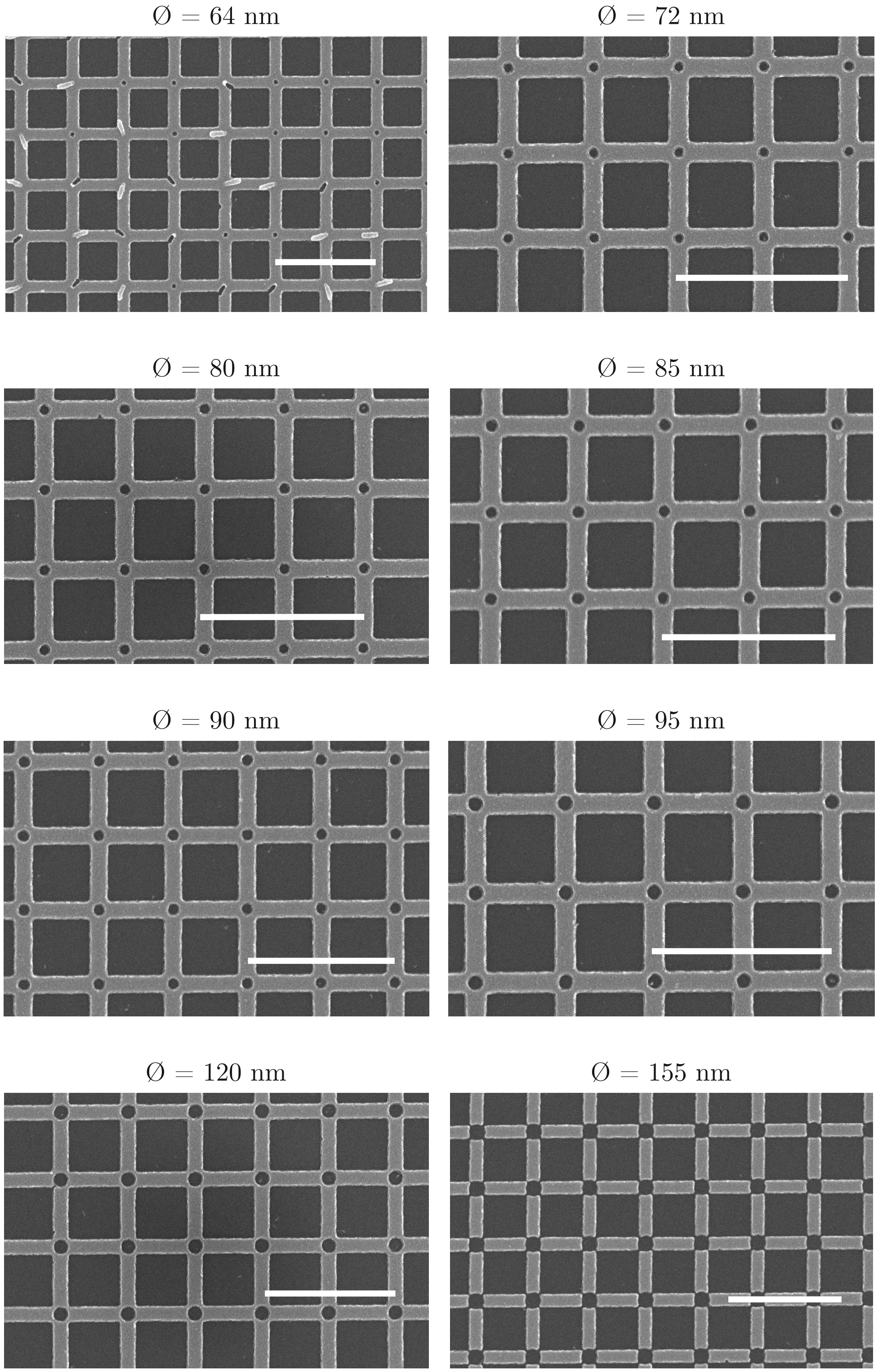

Figure 2.3: SEM images of part of the lattices with different hole diameters. All other lattice parameters were: width of the islands 100 nm, the distance from center of the vertex to vertex is 500 nm and thickness is 25 nm. All lattices are made from 30×30 vertices. The scale bar is $1\,\mu$m.

2.2. Measurement and data analysis

After the sample is fabricated and demagnetised, magnetic imagining of the resulted spin configuration needs to be conducted. The technique that suited best our needs is *magnetic force microscopy* MFM.

2.2.1. Magnetic force microscopy

MFM is one of the *scanning probe microscopy* (SPM) techniques based on measuring the local property of the sample by detecting the interaction between a magnetic probe and the magnetic stray field emanating from the magnetic structures.

Even though MFM can yield quantitative results, our measurements were done to acquire qualitative information about the samples from which the spin configuration of all lattices can be derived.

Acquiring qualitative data

Since our modified lattice for the kagome and the square systems are connected, we are not measuring the stray field of individual nanomagnets but the domain wall (DW) at each vertex site. From these domain walls, we can estimate the spin configuration of all three (in the case of kagome lattice) or four (in square lattice) connected nanomagnets.

To determine the spin configuration from the DW's shape and intensity, we first run MuMax^3 simulations to see how specific spin configurations form the stray field. The examples of possible DW shapes are shown in Figure 2.4. The domain walls can be rotated, and the micromagnetic texture can be reversed, but in principle, these examples represent all possible observable DW types.

In the kagome lattice, there are only two types of DWs. The low-energy ground state spin configuration is shown in Figure 2.4 a), where the magnetisation split around the notch. The high-energy spin configuration is the configuration where the magnetisation goes around the notch, shown in Figure 2.4 b). The simulated MFM signal for the ground state configuration results in a symmetric "heart shape" like the stray field. This DW shape is also measured by MFM, recognisable by its symmetry but mainly by no spike in intensity. On the other hand, the high-energy spin configuration is asymmetric both in simulated MFM and real measured signals. However, mainly the change in intensity in one part of the DW and the presence of the opposite (black/white) colour in the DW can be observed.

The square lattice has more types of possible DWs. The Type I domain wall is shown in Figure 2.4 c). This domain type is formed by spin configuration where two spins point into and two outside the vertex. The first neighbours (nanomagnets connected at an angle of 90°) have a "head to tail" spin orientation, and the domain wall have a characteristic "bow-tie" shape. This DW also has the lowest contrast of all types possible in our modified lattices. Therefore especially with large scans, this type of DW is often undetected or very poorly visible compared to other possibilities. There are only two ways this bow-tie DW can look: the light bow tie is oriented horizontally or vertically.

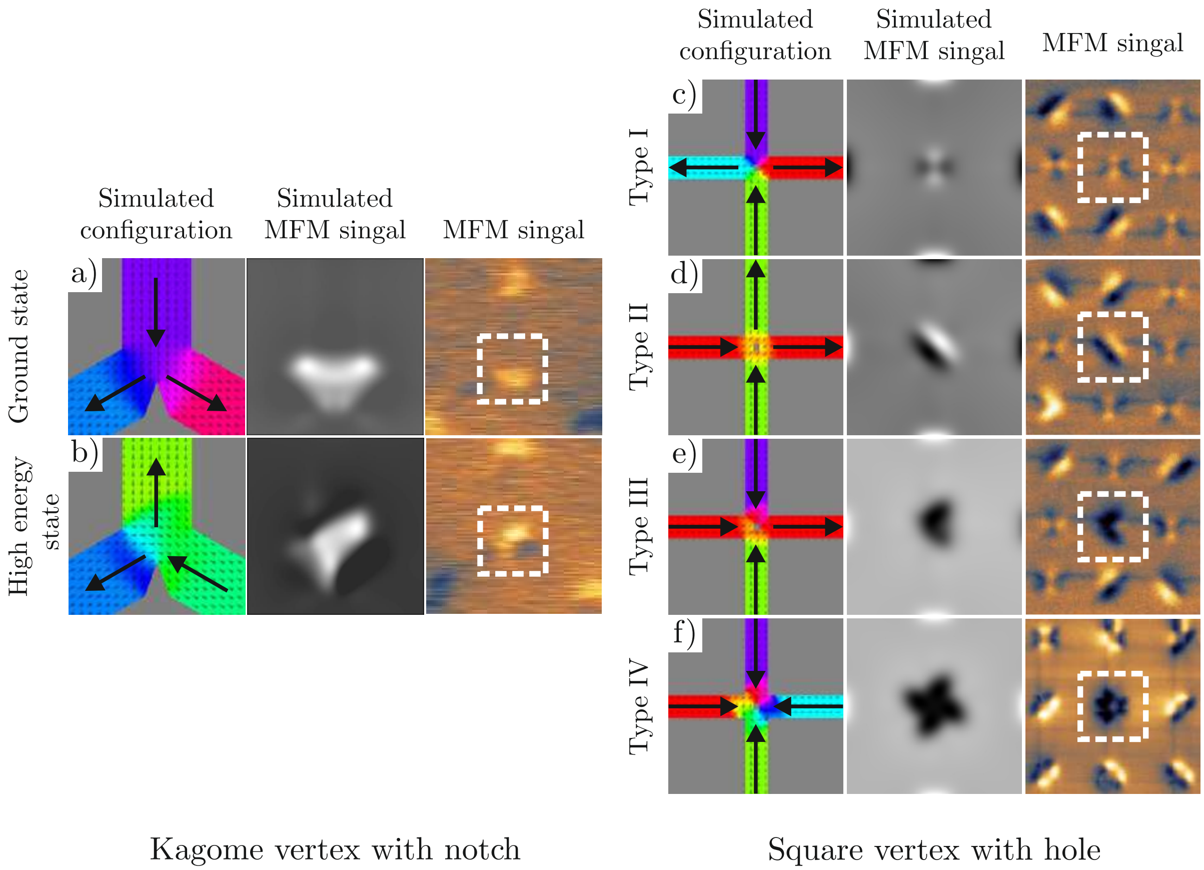

Figure 2.4: Comparison of simulated spin configuration and resulting domain wall signal with real measured MFM signal of the kagome vertex with notch with a) ground state spin configuration, b) high-energy spin configuration, and the square vertex with hole for c) Type I, d) Type II, e) Type III and d) Type IV spin configuration.

The Type II spin configuration is also made from two spins pointing inside the vertex and two outside, but the second neighbours now have a "head to tail" orientation. This DW is, therefore, polarised and has a characteristic two-colour ellipse-like shape. Contrary to Type I, Type II has a strong magnetic signal in simulations and real measurements. There are four possible spin configurations resulting in Type II DW. The ellipse can lean to the right or left side, and the white part can be both on top or the bottom of the ellipse.

The Type III configuration is made from three spin pointing inside or outside the vertex. Type III is a transverse domain wall, and there are eight possible spin configurations forming Type III with "heart shape" DW. Four configurations where one spin is pointing in and four where one spin is pointing outside of the vertex.

Type IV forms the DW, where all four spins point in or outside the vertex. There are only two possible ways spins can make Type IV DW, the four-in or four-out configurations.

It must be said that both Type I and Type IV configurations in our connected lattices have out-of-plane magnetisation at the centre of the vertex. Therefore these two types would have high-energy, and without the hole defect at the centre of the vertex, they would be unstable. Therefore, removing the area where this out-of-plane magnetisation would appear helps us stabilise these configurations. However, even with the centre removed in the vertex, the Type IV have much higher energy than the rest of the types. The only real space image of stabilised Type IV vertex visible in Figure 2.4 f) has been captured but only on the lattice with so many defects, making it unusable for research. However, these defects also made stabilising this rare configuration possible.

The proper discussion about the defects at the vertex site and the energies of individual DW will be discussed in Chapter 3 for the kagome lattices with notches and Chapter 4 for the square system with holes.

There are examples of how the AFM/MFM measurement outputs look for both types of lattices, as shown in Figure 2.5. AFM and MFM outputs were analysed and pre-treated with Gwyddion data processing software. The AFM outputs can give us information about the quality of the surface (whether there are some impurities) and the completeness of the lattice. It can be seen that in the kagome lattice, there is a nanomagnet missing in the bottom right corner. Except for the quality of the lattice, the AFM measurement does not provide any information about the spin configuration; however, knowing the topology defects can explain some unusual magnetic contrast in MFM measurements. The white bar indicates the length of $3\,\mu$m. Depending on the sharpness of the tip and on the lattice parameters, hole defects can be observed. On the other hand, in kagome lattices with notches, the notches are often hard to observe because the lattices are quite large, and to acquire many results, the measurement was done with relatively fast scanning and a large step size. Measurement was always set up to acquire the highest quality MFM images within a reasonable time frame (each measurement took around 50 minutes).

The interaction between the magnetic probe and the stray field of the sample is measured by the phase change of the probe's oscillation. Therefore the false colour scale shows the change in degrees. Where there are negative phase changes, the tip is attracted by the lattice via the magnetic field and vice versa for the positive changes. We are not measuring the direct magnetic orientation in the lattice but its interaction with the tip. Therefore if the tip was magnetised in the opposite direction, the measured contrast would also be reversed.

From the shapes of the measured DW in the MFM image, the spin configuration across the lattice can be determined as shown in the bottom panel of Figure 2.5.

The spin configuration of the square lattice is accompanied by the colour visualisation of the individual types of vertex configurations. The analysis can be done by hand, but it is a time-consuming process where many mistakes can be made. For this purpose, an in-house build software and scripts were programmed by Ioan-Augustin Chioar (PhD 2015), Yann Perrin (PhD 2016) and Vojtěch Schánilec.

2.2.2. Acquiring quantitative data

After measuring the spin configuration, the analysis is done to determine whether the system is at- or out-of-equilibrium, how fitting the physical framework (Hamiltonian) used in describing the system is, and what phase within the predicted thermodynamics profiles the system captures.

The process of the spin configuration analysis we use in our research is described in the following paragraphs.

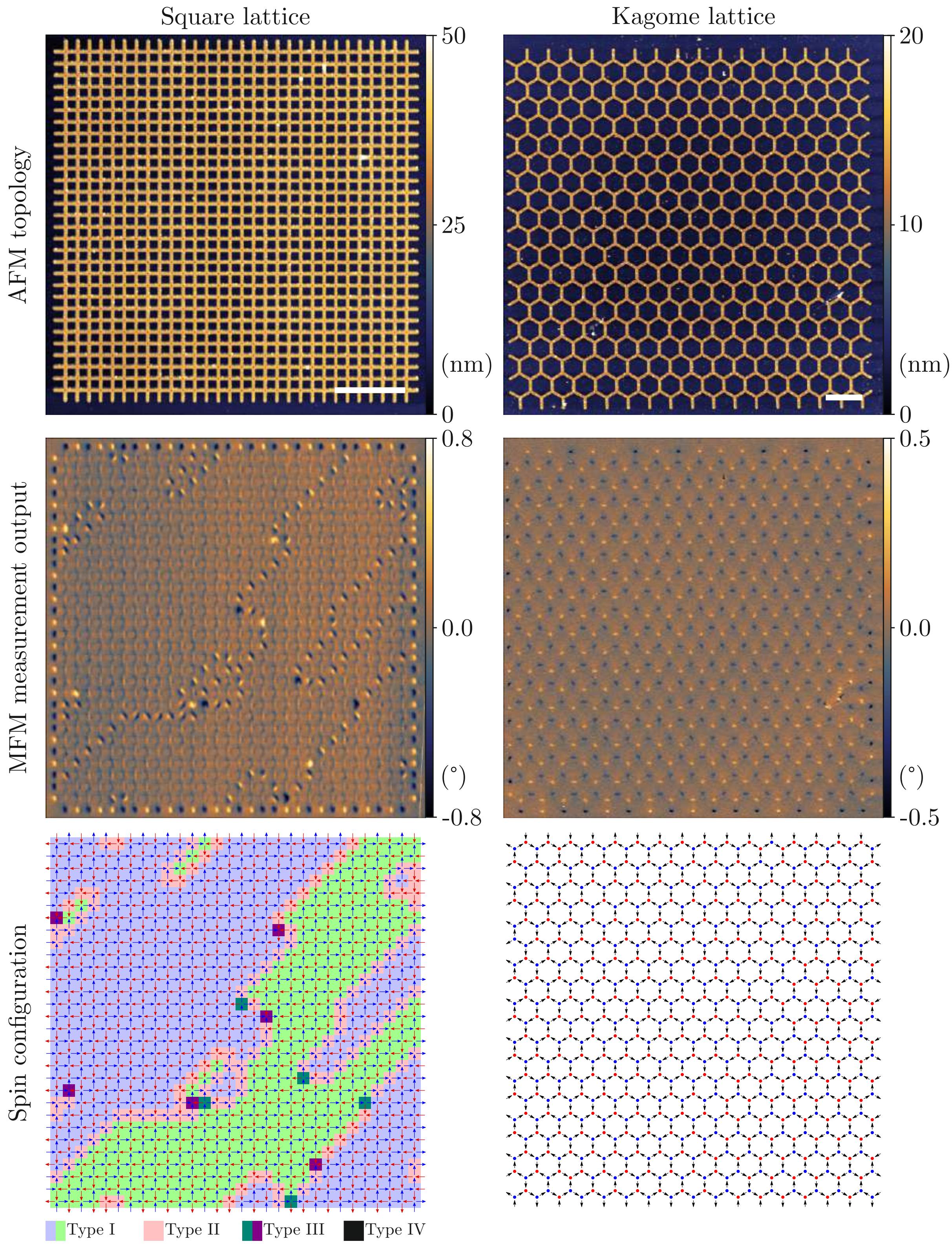

Figure 2.5: An example of measurement output from AFM and MFM on a square system with holes and kagome with notches. In the top panel are topographies of the lattices acquired with AFM. The white bars indicate the length of $3\,\mu$m. In the middle panel, MFM images show the domain wall formation at each vertex site. The bottom panel shows the visualisation of the spin configuration for the measured lattices.

Pairwise spin correlation

One of the type of analysis calculated from the real space images is the computation of the pairwise spin correlations. The correlations present a convenient way to see how the state of a given spin determines any other in the lattice. Pairwise correlations between the spin $\boldsymbol{S}_i$ and $\boldsymbol{S}_j$ are calculated as:

$$C_{ij} = \langle \boldsymbol{S}_i \cdot \boldsymbol{S}_j \rangle \,, \tag{2.1}$$

where $\langle\rangle$ indicates that the scalar product is averaged over all pairs of spins. It is particularly useful to compare the pairwise correlations calculated from the experiment $C_{\alpha j}^{\mathrm{exp}}$ with the correlations predicted by simulations. Monte Carlo simulations can be used to calculate these correlations $C_{\alpha j}^{\mathrm{MC}}$ for any desired Hamiltonian. Correlation coefficients are usually temperature dependent. To see if the measured spin configuration is, in fact, in-equilibrium and captures the physic of the predicted model, it is helpful to use the spread-out function defined as:

$$K\left(T\right) = \sqrt{\sum_j \left[C_{\alpha j}^{\mathrm{exp}} - C_{\alpha j}^{\mathrm{MC}}\left(T\right)\right]^2}. \tag{2.2}$$

By finding the minimum of this spread-out function, the effective temperature of the measured system can be estimated. If all experimental correlation coefficients fit within the deviation of the simulated coefficients, the system seems to be in-equilibrium.

If the experimental and simulated coefficients do not match, it can be caused by the following things:

- The measured system is not in thermal equilibrium.
- The system is in equilibrium, but the simulations were done with the wrong Hamiltonian, and therefore the physic of the system is not the same as the simulated one.

Magnetic structure factor

Another way to represent the spin configuration and order is to calculate the *magnetic structure factor* (MSF). MFS is obtained by calculating the Fourier transformation of pairwise spin correlations. The MSF shows the magnetic diffraction patterns associated with the real space magnetic state. Similarly to comparing the correlation coefficients with the predicted outcome, the MFS can be used to identify in which phase the measured sample is. These patterns are similar to the diffraction patterns acquired by neutron diffractions on spin ice crystals.

All MSF calculated for the square spin systems are done by Yann Perrin's code developed during his PhD studies. A deep description of how MSF is calculated is described in Perrin's PhD thesis [7]. Examples of how the MSF analysis can distinguish differences even in the configurations with the same or similar vertex populations can be seen in [8].

Chapter 3: Artificial kagome spin system with notches

One of the ways how to transform a 3D spin ice crystal into a 2D lattice is to use vertex projection. This transformation results in two-dimensional kagome geometry that will be the main focus of the following sections. In this summary only the realisation of kagome models will be discussed in 3.1 as well as the challenges tied with probing the artificial kagome spin systems are discussed in sections 3.2 and 3.3. The solution we propose how to overcome them will be introduced in section 3.4.

3.1. Artificial realisation of kagome models

Artificial systems are the perfect tool for probing exotic properties of matter, which would be hard or impossible to study otherwise. The idea to fabricate two-dimensional lattices of interacting nanomagnets disconnected [3] or connected [1] designed to capture the physics of frustrated systems opens a door for a wealth of studies on spin systems. The main advantage is having systems which can be probed in real space with imaging techniques. This advantage allows us to study the local configuration of each object (such as spin orientation or ordering of magnetic charges), and all global properties (spin-spin correlations, magnetic structure factors) can be calculated.

With improvements in EBL techniques, it is now possible to design arrays of small magnetic particles at will. If the nanomagnets are small enough, they are single domains and, therefore, can be counted as pseudo-Ising variables[1]. Anisotropy axis, which determines the orientation of such Ising variables, can be controlled by the shape of the nanomagnet.

There are two main approaches how to fabricate artificial kagome spin lattice with interacting single domain nanostructures. It can be built up from nano-magnets with out-of-plane magnetisation as seen in Figure 3.1 a). Nanomagnets with out-of-plane magnetisation are placed at the apex of each triangle in the kagome lattice (blue background layout). In this schema, orange represents magnetisation up and brown down. The second possibility is to use nanomagnets with an elongated shape and in-plane magnetisation as it is shown Figure 3.1 b).

At first glance, it might seem like systems shown in Figure 3.1 can perfectly capture the physic of the short range models. The following works proved that long range interactions play a significant role and are hard to suppress.

The first experimental work of Tanaka et al. [1] showed that artificial kagome arrays with in-plane magnetisation tend to follow the kagome ice-rule and therefore resemble the behaviour of short range model of kagome systems. In Figure 3.2 a) there is Tanaka's MFM image of permalloy lattice. A magnetic domain observation at each vertex site shows no ice-rule-breaking configuration presence. This system might seem like a good candidate for capturing the physics of the short range model, but since nanomagnets interact via

[1] A small single domain nanomagnet will always have a curl of its magnetisation at the edges - this is a feature that is usually neglected. Thus, the nanomagnet's magnetisation can be considered an Ising spin-like variable.

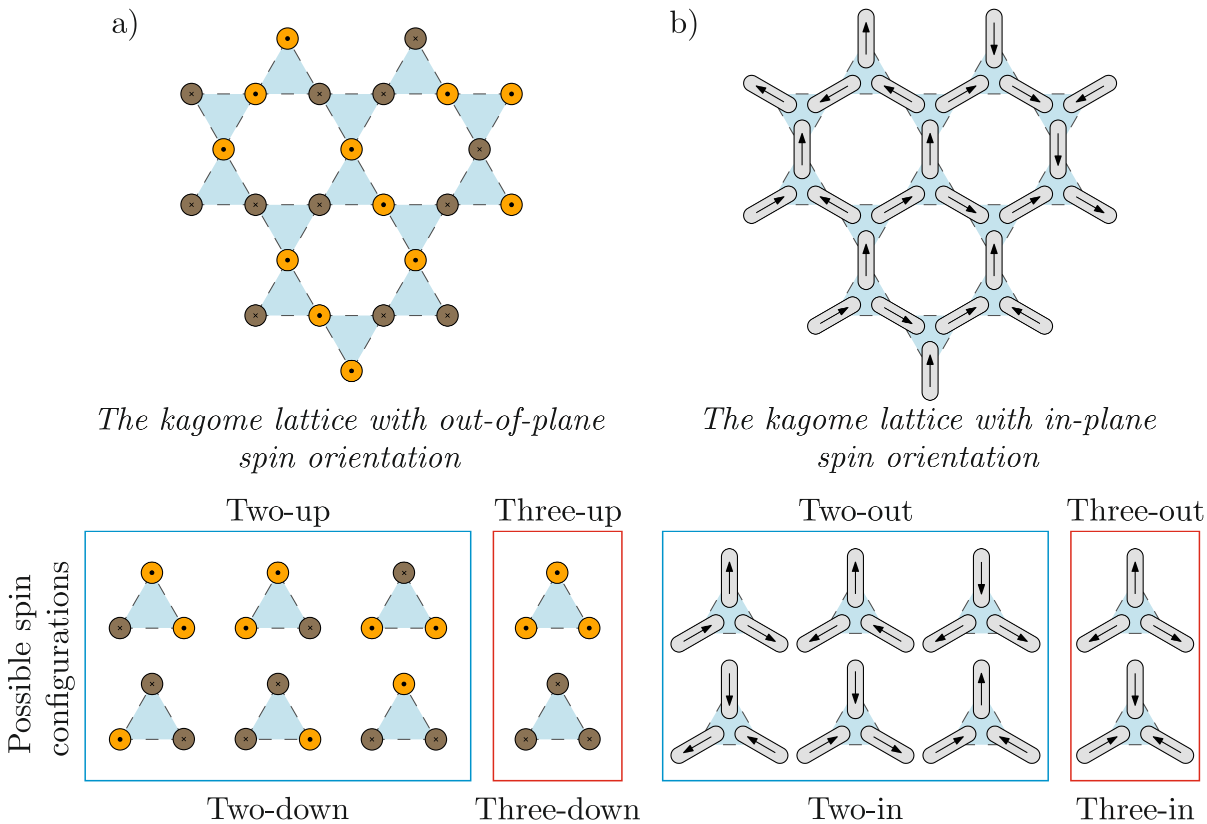

Figure 3.1: a) Nanomagnets with uniform out-of-plane magnetisation up (orange) or down (brown) placed on the apex of kagome lattice geometry. b) The kagome lattice made by nanomagnets with in-plane magnetisation. For both lattices, there are eight possible spin configurations of each of the vertices. These configurations can be divided into two groups: The first group follows the kagome ice-rules, and only two spins always point in the same direction (two-up/two-down or two-in/two-out of the vertex). In the second group, there are high-energy spin configurations where all spins point in the same direction (three-up/three-down or three-in/three-out of the vertex).

long range dipolar interactions, it is not the case. Qi et al. demonstrated that the ice-like physics of such structures could not be described using short range Hamiltonian [9].

Another possibility is to fabricate lattice with nano-discs with out-of-plane magnetisation as Chioar et al. did [10]. In Figure 3.2 b) you can see the magnetic contrast of TbCo nano-discs that gives the local directions of magnetisation. Nevertheless, by analysis of correlation coefficients and magnetic charges correlation, Chioar et al. proved that this system, too, is affected by long range interactions.

At this point, many works are building on Tanaka's founding and studying long range dipolar kagome spin ice. But there are promising attempts to design systems where the long range interactions and effect of father-neighbour couplings are minimized[2] in artificial kagome dipolar Ising antiferromagnet by using a mixture of out-of-plane and in-plane magnetisation regions [11] as can be seen in Figure 3.2 c) where redly highlighted areas have out-of-plane magnetisation, and they are connected to the areas with in-plane magnetisation (blue ones). White bar indites length of 500 nm in each of the images.

[2]Minimised but not eliminated.

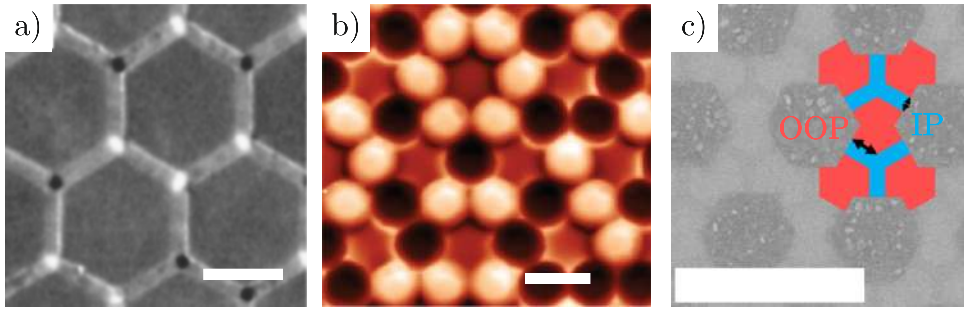

Figure 3.2: a) Pioneering work of Tanaka's showing MFM contrast of kagome dipolar spin ice permalloy lattice with in-plane magnetisation and kagome ice-rule obeying spin configurations taken from [1]. b) MFM image of the kagome dipolar Ising antiferromagnet Chioar's TbCo nanodiscs array with out-of-plane magnetisation taken from [10]. c) Artificial lattice combining the areas with out-of-plane magnetisation and in-plane magnetisation to reduce the effect of long range dipolar interaction within the system as proposed by Colbois et al. [11].

One of the challenges of studying artificial kagome dipolar systems is bringing them into their low-energy phases, mainly due to the effect of critical freezing at the SL1/SL2 border, where magnetic charge crystallisation occur.

In this work, we show how to bypass the intrinsic problem of freezing the dynamics simply and with our approach, we can access a priory dynamically inaccessible ordered ground state of kdsi and even fragmented spin liquid configurations.

3.2. Phases of the kagome dipolar spin ice

The interest in the kagome dipolar spin ice (kdsi) system arises from the fact that this system has a very peculiar phase diagram. The phases of kdsi are following: *Paramagnetic phase* (PM), *Spin liquid 1 phase* (SL1), *Spin liquid 2 phase* (SL2) and *Long range order phase* (LRO).

Thermodynamic evolution of entropy and specific heat of kagome dipolar spin ice system is shown in Figure 3.3 calculated using Monte Carlo simulation by Canals et al. [12]. Both of the quantities are plotted dependent on T/J_{NN}, where T is the temperature of the system and J_{NN} is the coupling strength constant between nearest neighbours. As the temperature decreases the systems evolve via crossover (orange line in Figure 3.3) from high-temperature paramagnet into SL1 and the system starts to correlate. Further decrease in the temperature force the system to undergo a phase transition from SL1 to a fragmented SL2 phase. During this transition, there is an immense loss of entropy (which will be discussed further in the text closely) and a spike in specific heat. If the system is cooled enough, the second phase transition occurs, and the system ends up in the ground state long range order configuration. Black dashed lines highlight both phase transition temperatures.

The best way to fully describe the difference between each phase is to look at the spin configurations, magnetic charge configurations and spin dynamic constraints. For that purpose, dedicated figures comparing the following properties for all phases are provided:

1. *Spin configuration* - whether the spins are ordered/disordered and correlated/uncorrelated. In Figure 3.4 you can see an example of: a) the spin configuration and b) the average spin configuration corresponding to each phase. An easy way to visualise spin ordering in real space is to show which simple loops (the smallest possible loops are made from six spins) have a closed flux of spins. A green dot will highlight these loops. However, this property is best visualised by calculating the correlation coefficients and magnetic structure factors, which give us information about how the spins correlate. Both correlation coefficient and MSF temperature dependence are shown in Figure 3.5.

2. *Magnetic charge*. This property is visualised by red or blue coloured circles for positive or negative charges. Small circles represent ± 1 charges, corresponding to two-in/two-out spin configuration and large circles ± 3 corresponding to high-energy three-in/three-out configuration. Examples of possible charge configuration and average charge configuration for each phase are shown in Figure 3.4 a) and c), respectively.

3. *Spin dynamic constraints* - in each individual phase, different constraints of the spin dynamics arise from both charge and spin configuration energy minimisation requirements. These dynamic constraints are shown in Figure 3.6.

Each of these three aspects will be discussed individually for every phase in the following paragraphs.

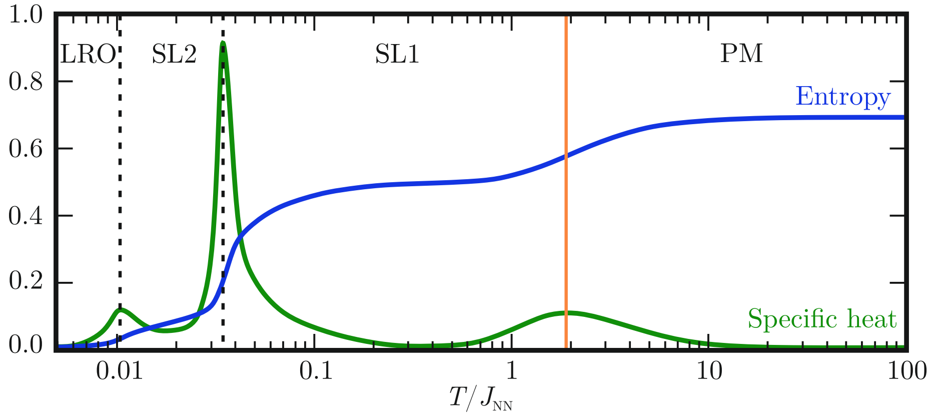

Figure 3.3: The simulated temperature dependencies of the entropy and specific heat of the kagome dipolar spin ice system. T/J_{NN} is the temperature of the system normalized to the nearest neighbour coupling strength. Crossover temperature between PM and SL1 phases is coloured orange, while phase transition temperature between SL1/SL2 and SL2/LRO phases are black dashed lines. Taken and edited from [12].

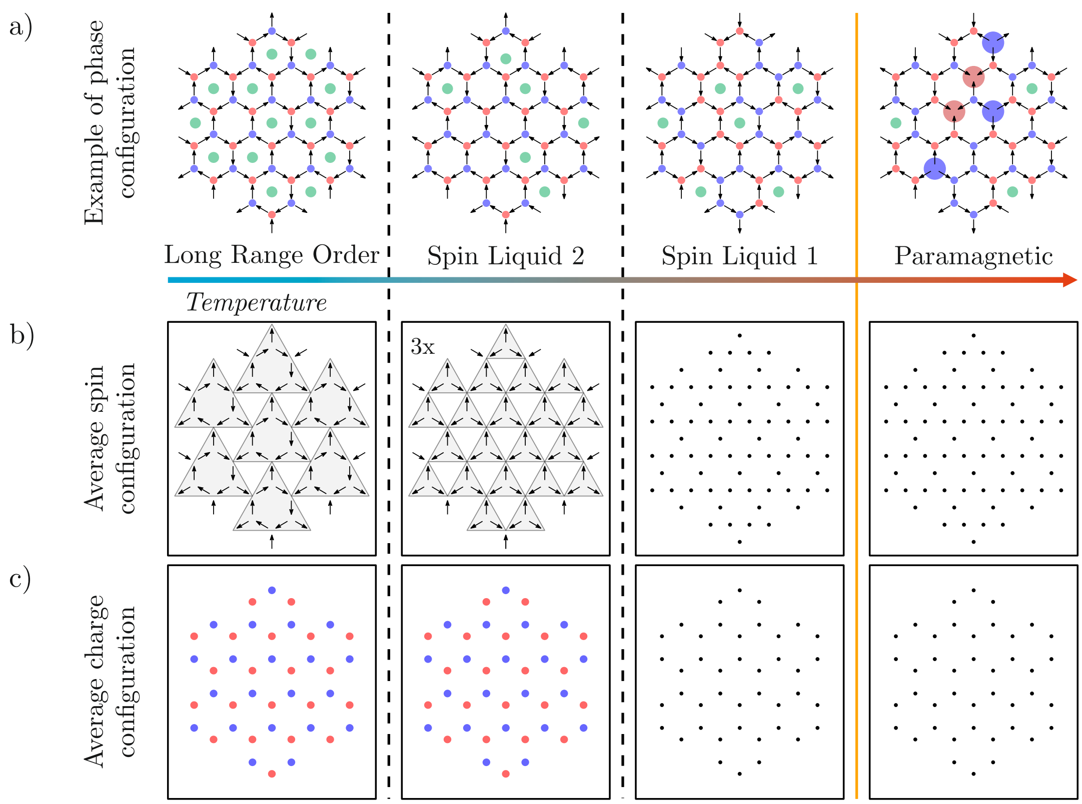

Figure 3.4: a) Examples of possible spin and magnetic charge configurations. Red and blue dots represent magnetic charge and the green dots represent hexagons with closed magnetic flux. b) Average spin configuration, where arrows represent the mean value of spin after averaging. The length is zero for the PM and SL1 phase, 1/3 for the SL2 phase and 1 in the LRO phase. The shaded triangles show the spin unit cell. c) Average magnetic charges, where the blue and red dots represent the mean value of the magnetic charge. While in PM and SL1, the value is zero on average, in SL2 and LRO, phase magnetic charge is ordered with alternating value ± 1. Taken and edited from [13].

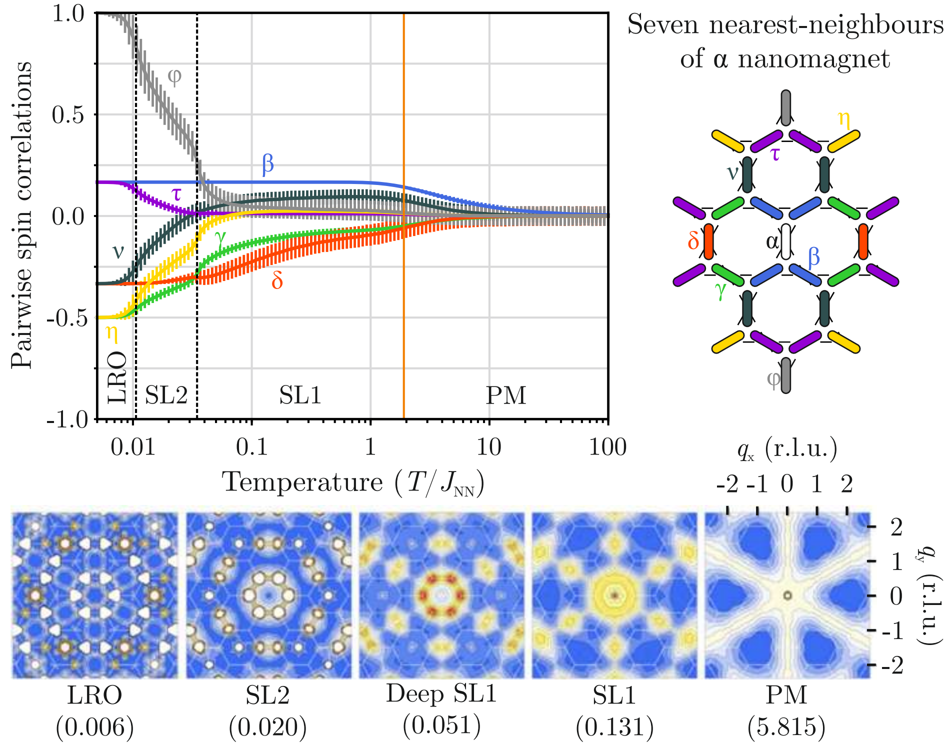

Figure 3.5: Monte Carlo simulations of temperature-dependent pairwise spin correlations of the first seven neighbours to α. The orange line indicates the crossover temperature between PM and SL1, and the black dashed lines mark the temperature of phase transitions between individual phases. In the bottom panel, MSF is calculated for different effective temperatures (shown in brackets below) belonging to each phase. MSF are taken and edited from [12]. MSF images show how system goes from disordered (indicated by diffused background) PM phase into perfectly ordered (indicated by intensive Bragg peaks) LRO phase.

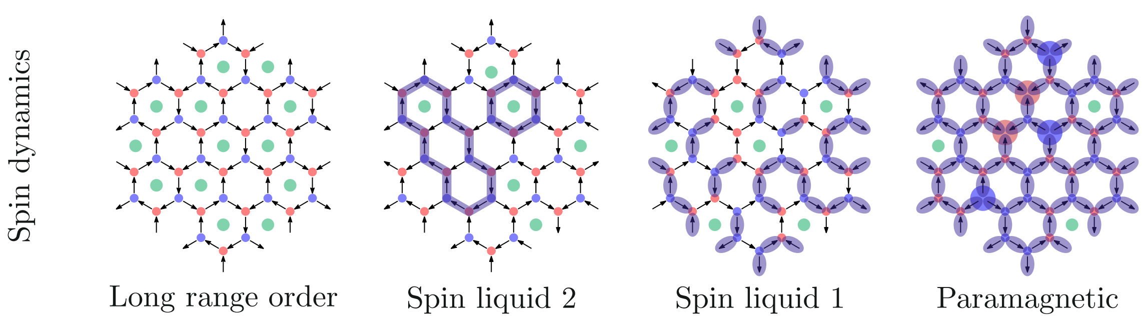

Figure 3.6: Schematics of the possible spin dynamics in all kdsi phases. Spins that are allowed to flip are highlighted in purple frames. In PM, all spins can flip freely since there are no charge or spin constraints. In SL1, only some spins can flip rest of the spins are frozen as flipping them would lead to the kagome ice-rule-breaking three-in or three-out spin configurations. In the SL2 phase, another constraint is present as magnetic charge crystallisation occurs; therefore, the spins can only flip if the whole loop containing the spin switches. If not, the charge ordering would be broken. In the LRO phase, everything is perfectly ordered, and no spins are allowed to flip.

Paramagnetic phase

PM phase is the highest energy phase of kdsi. An example of the spin configuration of the PM phase can be seen in Figure 3.4 a). In this phase, the temperature T of the system is much higher than the coupling constant between the nearest neighbour J_{NN} e.i. $T/J_{\mathrm{NN}} \gg 1$. There are no constraints on spin dynamics, and all spins are allowed to change their orientation without any limitation[3]. In this phase, spins are uncorrelated, as is proven by Monte Carlo simulations in Figure 3.5 where all pair-wise correlations fluctuate around zero and MSF shows only diffused background. Even high-energy spin configurations are possible; hence vertices with magnetic charge +3 (large red circle) or -3 (large blue circle) can be observed. Due to the constant spin flips leading to random magnetic charge configurations, the average spin and magnetic charge configuration are zero, as is shown in Figure 3.4 b) and c).

Spin liquid 1 phase

As the temperature decrease to values $T/J_{\mathrm{NN}} \sim 1$, the system evolves into the SL1 phase. The spins start to correlate as Monte Carlo simulations show in 3.5, and in the MSF image, we can see how fingerprints of correlations start to emerge. Therefore this phase is disordered but correlated as one would expect from the spin liquid. There are no ± 3 magnetic charges since the effect of coupling strength of the nearest neighbours starts to have more power over the dynamic of the spin; therefore, in Figure 3.4 there are only ± 1 magnetic charges and no visible spin ordering. The spins still fluctuate but only if the resulting configuration follows the kagome ice-rule, and thus average spin and magnetic charge configuration is zero. As it can be seen from the evolution of correlation coefficients and MSF images (see changes in-between higher temperature MSF of SL1 and low temperature deep SL1 MSF), SL1 phase correlations coefficients are temperature dependent.

Spin liquid 2 phase

Further temperature reduction causes longer range couplings to correlate, and the systems undergo the first phase transition into the SL2 phase. Even though most of the residual entropy is released, as is shown in Figure 3.3 SL2 phase is still macroscopically degenerated [14, 15]. In spin liquid 2 phase spins develop stronger pair-wise correlations. Moreover, a puzzling behaviour of the system appears. On the one hand, magnetic charge crystallisation occurs, and ± 1 charges periodically alternate across the system. This crystallisation indicates strong spin ordering, but on the other hand, spins are still highly fluctuating. It must be said that there is no magnetic charge degree of freedom encoded in the system's Hamiltonian. Therefore magnetic crystallisation seems to emerge out of nowhere.

However, the spin fluctuation now must obey not only the kagome ice-rule but also magnetic charge constraint, meaning that spins are only allowed to flip in a way that will not disturb the charge ordering. Such flipping can be achieved only if spins fluctuate in collective loop spin flips, as shown in Figure 3.6. Spins are ordered and disordered at the same

[3] Spins are still Ising variables, so they only fluctuate between two possible orientations.

time. Therefore, diffused background in MSF coexists with rising Bragg peaks signal as is shown in Figure 3.5. This behaviour of spins is called *spin fragmentation* because each spin can be considered fragmented into a static and dynamic part of itself. Signatures of spin fragmentations have been detected experimentally [16, 17] and even observed in real space measurement on a fraction of the sample [12].

The first partial capture of the SL2 phase in real space in a portion of the system was captured by Canals et al. [12].

Long range order phase

As the system temperature drops to the level of the second phase transition from SL2 into the LRO phase, almost all the residual entropy is released, and the system enters its two-times degenerated ground state.

In the LRO phase, the spins are perfectly ordered and therefore highly correlated, as shown in Figure 3.5. Example of the LRO phase in Figure 3.4 a) shows the perfect ordering of smallest possible loops (six spins) with closed magnetic flux as visualised by the green dots. Average spin configurations are perfectly ordered while maintaining the magnetic charge crystal, which results in intense Bragg peaks in the MSF image as shown in Figure 3.5.

The first ever real space image of the LRO phase was measured by Gartside et al. [18] with a clever trick. They fabricated six hexagons of magnetic nanostructures and saturated the magnetisation in one direction. Using a high-moment MFM tip, they then reversed the spin orientation of chosen islands (blue ones) to form perfect LRO ordering.

3.3. Dynamical freezing

As mentioned, one of the main problems of probing low-energy phases of kdsi (or kdIa) systems is the critical slowing of spin-spin correlations as the system approaches the SL1/SL2 phase transition. There are two different contributions to the slow-down effect: critical slow down and single spin freezing.

Firstly, as with any phase transition, the system exhibit *critical slow down* near the phase transition. It takes the system more time to return to equilibrium, even after small perturbations or disturbances are made.

The second factor that causes the slow-down is freezing the single spin-flip dynamics. In Figure 3.7 result of the MFM measurement of the kagome lattice can be seen together with a spin and a magnetic charge configuration of zoomed section. The system was brought into this configuration via magnetic field demagnetisation. There are no three-in or there-out configurations, the magnetic charge is disordered, and the system is in the SL1 phase. If we look at the spin and magnetic charge configuration, we can see areas with a white and green background. These areas indicate patches of magnetic charge domains. The spins crossing the border of these patches are frozen; they cannot flip because it would introduce a three-in or a three-out defect within one of those patches. The inability of spin flips means that the domain walls are frozen and cannot evolve, and the system is frozen in this configuration. The patches of magnetic charges nucleate randomly all over the system and can only grow if the neighbour patch vanishes and is absorbed into the growing patch. For this annihilation of a large magnetic charge patch, first, one of the border frozen spins would need to flip - leading to a high-energy configuration. Only after that could the spins co-creating this three-in/three-out defect flip and bring the whole lattice into a lower-energy state, closer to the SL1/SL2 phase transition. The deeper in SL1 the system is, the less probable such transient high-energy excitations are.

The only possible single spin flips are those which annihilate the patch by itself. Examples of all such spins are highlighted in Figure 3.7 with black ellipses surrounding them.

Therefore the dynamical freezing is a consequence of significant energy barriers separating quasi-degenerate configuration, and the system cannot find a more energetically favourable state.

The freezing of dynamics is an intrinsic, model-dependent mechanism; thus, it is an ever-present slowing factor and must be bypassed with external effects to reach the low-energy phases. Dynamical freezing is not occurring only in the dipolar kagome ice but is affecting all systems where loop dynamics drive the low-energy manifolds.

Probing the low-energy manifolds is still challenging in the ice models [17] if possible. Therefore the LRO and SL2 phase in the artificial dipolar kagome ice have never[4] been observed and studied in real space.

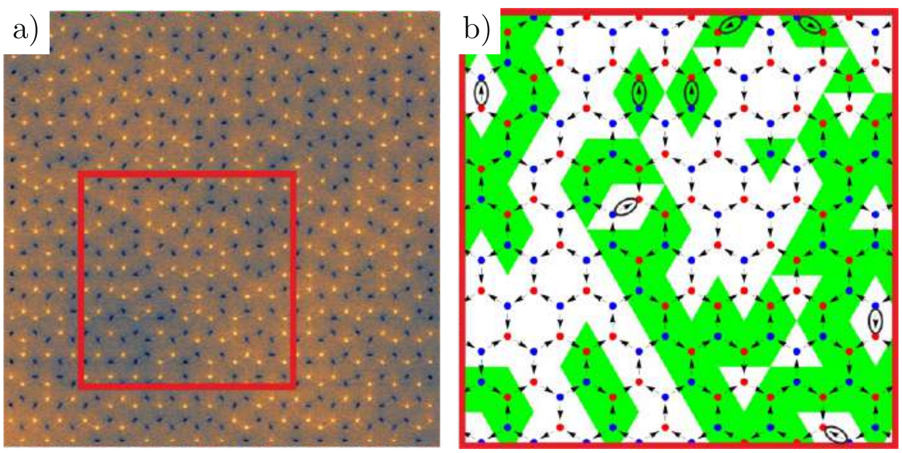

MFM image of SL1 phase

Spin configuration and magnetic charge of framed area

Figure 3.7: a) MFM image of permalloy lattice with connected nanoisland in SL1 phase with a red framed zoom section on a random part of the lattice. b) Spin configuration of zoomed area together with a corresponding magnetic charge. The white and green area indicates two opposite patches of magnetic crystal. Only highlighted spins are allowed to flip. All other spins are frozen. Taken and edited from [13].

[4]Only exception is research done by Gartside et al. [18]. Although they manually write the configuration spin by spin with MFM tip

3.4. Modified artificial kagome lattice with notches

In this work, we demonstrate, numerically and experimentally, one possible way to bypass dynamical freezing in artificial kagome ice. We are reproducibly and efficiently able to bring the system into any desired microstate satisfying the ice-rule. Specifically, we can force the system to form any spin and magnetic charge configuration of SL1, SL2 and LRO phases.

Artificial spin ice systems are typically build of small single domain nanomagnets, as shown in Figure 3.8 a), which are usually considered to be Ising pseudospins [19–22], and their micromagnetic texture is neglected. To the contrary, the strategy presented in this work relies heavily on micromagnetism as a key ingredient. Vertices in our systems are connected with a notch at each vertex, as shown in Figure 3.8 b). This notch locally lifts the system's degeneracy and prefers a specific spin configuration. With this, lattice can be built up vertex by vertex with desired spin configuration imprinted within its topology.

By tuning with geometrical parameters such as length or width of the nanomagnet and position, top angle or depth of the notch, we can tune the total energy of the micromagnetic texture at the vertex site.

The fabricated system differs from a conventional kagome lattice in a way that now it is not an assembly of interacting nanomagnet. Instead, the system can be viewed as a single object - magnetic grid where the main driving force is no longer two-body interaction between all pairs of spins in the system but the micromagnetic texture at the vertex site. Therefore, we consider this system not to be a spin model but a vertex model.

The illustration of the difference between these models is in Figure 3.8, where spins (represented by arrows) in a) can interact via dipolar interactions even with farther neighbours same as an array of interacting nanomagnets. However, in the vertex model in b), vertices represented by *the puzzle pieces* only affect their nearest neighbours via connections they share.

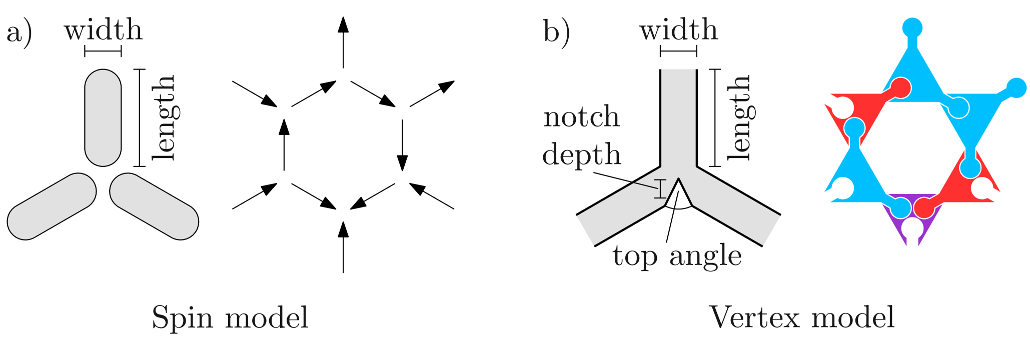

Figure 3.8: a) Schema of kagome vertex formed by separated single domain nanomagnets described by length and width. The behaviour of such a kagome lattice is described as pseudo-spins interacting via dipolar interaction. b) Schema of the kagome vertex with connected island and notch with all important geometrical parameters highlighted. The driving force of systems with connected nanomagnets are micromagnetic forces at the vertex site, and the nearest neighbours are only affected by the connection they share - similar to *puzzle pieces*. Systems with this behaviour can be described well by the vertex model.

3.4.1. Magnetostatic effect of the notch

Changing the geometry of the artificial kagome spin system by adding the notch will break the symmetry of the vertex and lift the system's degeneracy. The six spin configurations that follow the ice-rule now break into two groups. Two of them now have lower energy than the four rest, as is shown in Figure 3.9 a). The total energy of the magnetic domain wall at the vertex site is in case of permalloy vertices the sum of the *exchange* and *demganetisation* energies. The energy E_1 of the vertex configurations in blue frames is lower than energy E_2 of the configurations in the red frames.

The notch size can be used as an external parameter to tune the total energy of E_1 and E_2 configurations. The energy dependence on the notch size and thickness of the structure is plotted in Figure 3.9 b). Grey, blue and purple data sets represent the energy of the E_1 configuration, and red, green and gold data sets are energies of E_2. When the depth of the notch is zero nm, the energy value for E_1 and E_2 is the same, but the energy spiting is visible as the notch goes deeper into the vertex.

The micromagnetic simulations were performed using Mumax3 code [23], with the following simulation parameters: The nanomagnets were 750 nm long, 250 nm wide and with three different thicknesses 5, 10, 25 nm. The depth of the notch varied between 0 and 300 nm with 50 nm step. The top angle of the notch is fixed to 30°. Since our experiment uses permalloy as magnetic material, the stiffness constant is set to 10 pJ/m, magnetocrystalline anisotropy is neglected, and spontaneous magnetisation is $8 \cdot 10^5$ A/m to best mimic the behaviour of real structures. The damping coefficient is set to 0.5. To limit the influence of numerical roughness mesh size of the simulations has been reduced to $2 \times 2 \times t$, where t is the thickness of the structure.

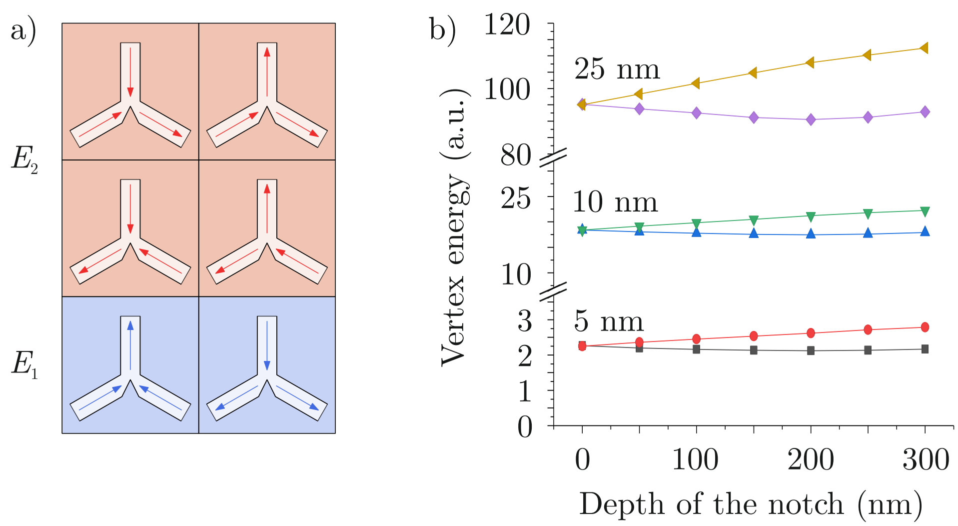

Figure 3.9: a) Six possible spin ice configurations in our modified lattice. Due to the presence of the notch, configurations in the blue frame have lower energy E_1 than energy E_2 of configurations in red frames. b) The vertex energy dependence on notch depth was simulated for three different thicknesses: 5, 10 and 25 nm. Grey, blue and purple are results for E_1 configurations, and red, green and gold data sets are energies of E_2. The energy gap between E_1 and E_2 always increases as the notch goes deeper into the vertex. Taken from [13].

For clarity, we define *the notch-rule* (a special case of ice-rule) that states that the vertices with notch prefer spin configurations with energy E_1. Large notches force the system to obey the notch-rule and to pick one of the two times degenerated configurations. However, if the notch is small, it slightly increases the probability of such a pick. With this knowledge, we can now build up vertex by vertex the whole lattice with the desired phase imprinted in its topology.

3.4.2. Imprinting the phases

To prove our concept, we fabricated several lattices with different phases of dipolar kagome ice imprinted into the topology. A series of kagome lattices with connected islands were made from permalloy material. The lattices were fabricated using EBL, and the resulting arrays consist of 250 nm wide and 1 μm long connected nanomagnets. The targeted thickness of the lattice was 15 nm. A notch was incorporated into every vertex site with a fixed 30 $^\circ$ top angle. The depth of the notch was constant in each lattice but varied from 50 to 250 nm in between different sets of lattices. To have better statistics and eliminate the effect of the edges, each lattice contains approximately 10^3 nanomagnets.

All the lattices were demagnetised using a magnetic field protocol similar to the protocol used in [16, 24]. The length of the demagnetisation protocol will be mentioned with all the results. The measurement was done with the MFM technique.

Examples of how we use the notch position for imprint individual phases are shown in Figure 3.10, where there are SEM images of a) LRO and b) SL2 phases with the addition of the graphics on how the spins and resulting magnetic charge would be ordered in both cases. The same procedure can acquire lattices with any thinkable ice-rule obeying spin configuration.

Imprinting the LRO phase is easy since all the spins have to be perfectly ordered. To achieve such ordering, the notches must be periodically placed all over the lattice. The tricky part is to figure out how the notches need to be placed on acquiring one of the possible SL2 phases. We run Monte Carlo simulations to acquire a possible spin configuration of the SL2 phase. From the output of these simulations, we draw the layouts with a semi-automatic procedure where notches are placed at the vertices in a way that will lead to the configuration matching the Monte Carlo simulations.

Experimental results of lattices with imprinted phases are shown in Figure 3.11. For each of the LRO, SL2 and SL1 phases, AFM topology and MFM magnetic contrast is presented in top and middle panels, respectively. Individual spin orientation can be acquired with a magnetic charge from MFM contrast, and both are plotted in the bottom panel. The topology of individual lattices and especially the positions of individual notches are hard to read. Therefore AFM images do not bring much information. For this reason, a further presentation of MFM measurement will not be accompanied by AFM topology but only with spin and magnetic charge configurations.

In Figure 3.11 a) lattice with LRO phase imprinted with the notch depth 200 nm shows almost perfect magnetic charge ordering in MFM image all across the lattice with a few exceptions at the edges. Domain wall dynamics cause these defects during demagnetisation. The length of the demagnetisation protocol used on this lattice was 7 days. In b)

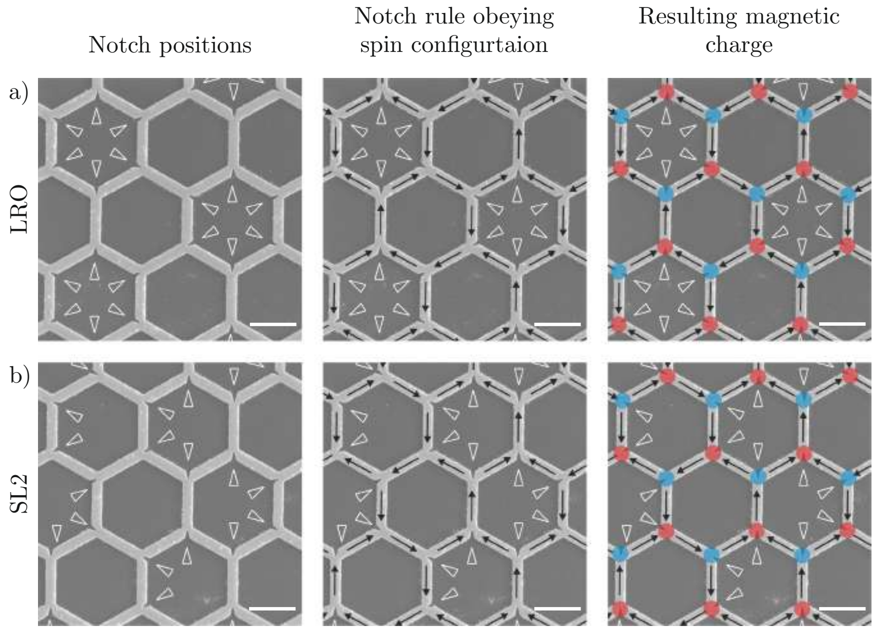

Figure 3.10: SEM images of two different lattices with notches. a) The LRO phase is imprinted into the lattice. Notch positions and orientations are periodic and white triangles highlight their position. Spins are perfectly ordered if they all obey the notch-rule, and the magnetic charge alternates from +1 to −1 all over the lattice. b) The SL2 phase is imprinted into the lattice, and positions of the notches are chosen, so the notch-rule spin configuration is one of the SL2 manifolds. The magnetic charge would also alternate in this lattice, but spins are not perfectly ordered. Black arrows indicate one of two possible ground state spin configurations of the lattices. White bars indicate the length of 1 μm.

lattice with SL2 phase is imprinted with notch size 200 nm and the 3 days long demagnetisation protocol. LRO and SL2 have almost perfectly ordered magnetic charges, which means that the spins followed the notch-rule, but a more complex analysis will be done further in the text. SL1 phase shown in Figure 3.11 c) has no notches, and therefore all vertices follow the ice-rule instead of the notch-rule, which leads to a disordered phase of SL1.

The lattices with imprinted phases are brought to their ground state with field demagnetisation protocol, which is a strikingly different approach than the one introduced in [18]. The desired spin order is not restricted to only a few hexagons but is observed across the lattice. The dynamical freezing described in section 3.3 is therefore efficiently bypassed, and the previously inaccessible phases of the kdsi model are easily imaged. This approach can be used to acquire any ice-rule obeying microstate.

3.4.3. Disadvantages of the notch presence

The ability to imprint any desired ice-rule-obeying configuration into our lattices comes with a price to pay. We are destroying the system's symmetry and changing the Hamiltonian using the notch defects. The effect of the changed Hamiltonian is discussed in the full version of the thesis. As a consequence of bypassing the dynamical freezing with our notch approach, we do not need the loop dynamics, and single spin flip events can reach

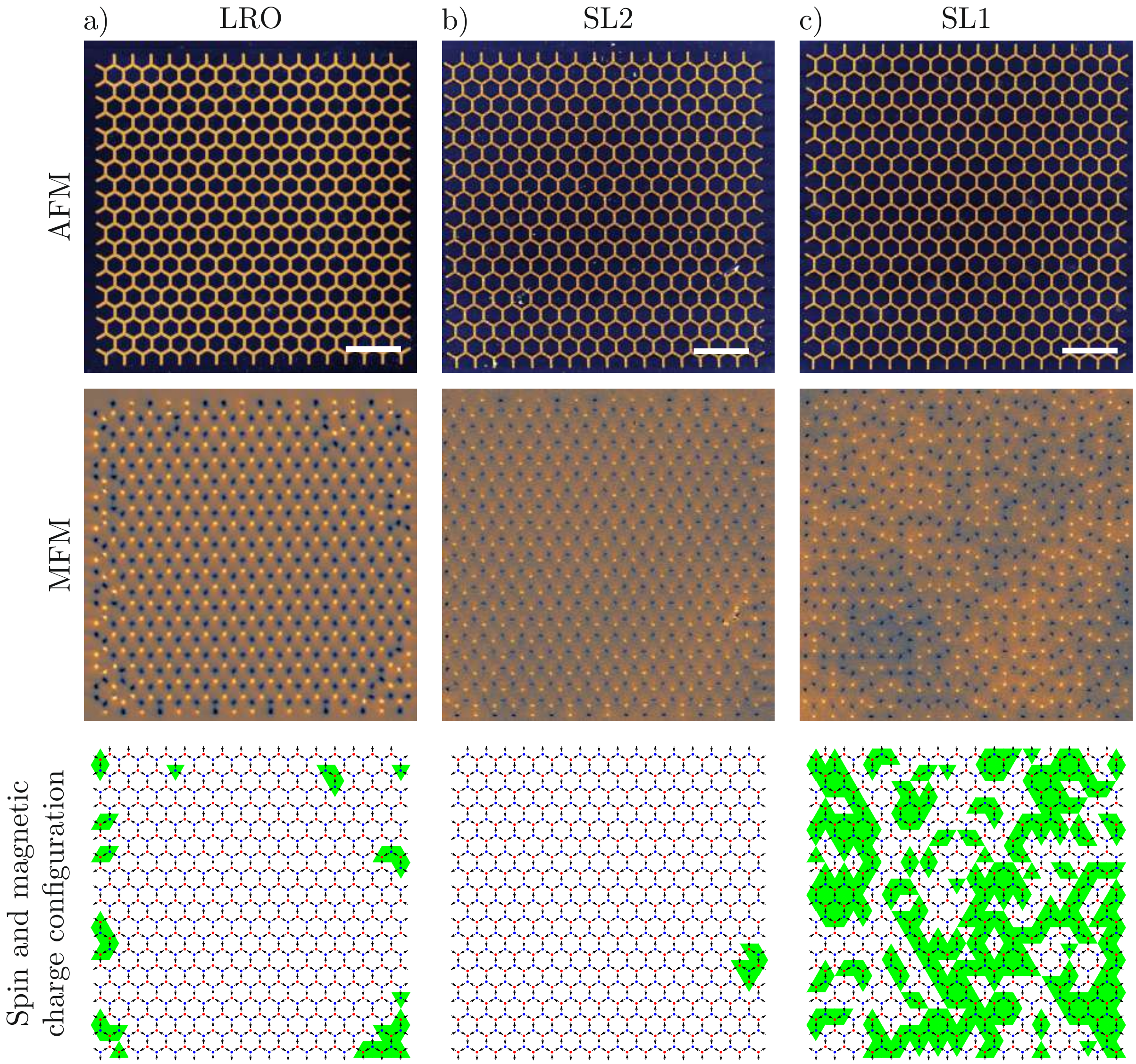

Figure 3.11: Examples of lattices with a) LRO, b) SL2, and c) SL1 phase imprinted. a) The MFM image shows almost perfect magnetic charge ordering in the LRO lattice. The reconstructed spin configuration shows perfect spin ordering following the notch-rule, with a few exceptions at the edge of the lattice. b) MFM image acquired by measuring SL2 phase shows perfect magnetic charge ordering and all spins except the three vertices in green patch perfectly follow the notch-rule. c) SL1 phase is exhibiting no charge ordering. Since no notch was used anywhere in the lattice, the ice-rule condition is obeyed. Spins are disordered, as well as magnetic charges.

the imprinted ground states. However, without any loop dynamics, we cannot properly probe the physics of the SL2 phase - we can only probe one imprinted microstate.

Surprisingly even though we changed the Hamiltonian of the system by imprinting the desired microstate, we were able to heat the system and measure configurations that have the same spin correlations corresponding to the higher effective temperature of the kagome dipolar spin ice. There is one puzzling question yet to be answered. How is it possible to observe correlation coefficients which almost perfectly fit the thermodynamic profile of KDSI, even with the changed Hamiltonian?

Chapter 4: Artificial square system with holes

The square geometry is a result of the edge projection of 3D pyrochlore crystal into 2D plane as shown in Figure 4.1 a) where spins with in-plane orientation are placed onto the square projection (blue lattice). Although it is possible to have a square model with out-of-plane magnetisation [25], for the simplicity of the explanation, this realisation can be omitted since the physics of our experiment is linked only to the models with in-plane magnetisation.

However, the edge projection destroys the symmetry of the system, unlike the vertex projection (resulting in kagome geometry), by making a distance shift in between the spins creating vertex as is shown in Figure 4.1 b). There are now two types of pairs of spins in the vertex. The nearest neighbours are the spins which are perpendicular to each other, and they have coupling strength constant J_1. The second nearest neighbours are parallel, and their coupling constant is J_2. The symmetry breaking is causing a deviation from the water ice and spin ice systems. Therefore, it poses a challenge that must be solved to regain the proper degeneracy expected from the spin ice systems.

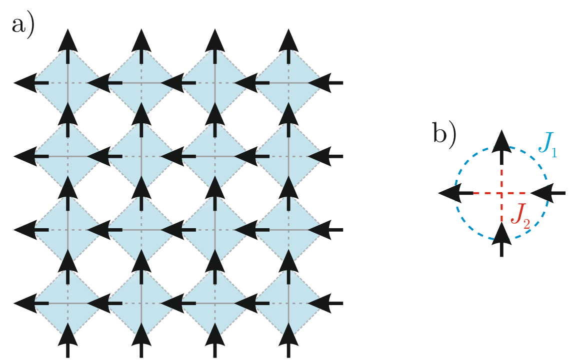

Figure 4.1: a) Square geometry results from the edge projection of pyrochlore crystal. The spins are placed at the apexes of the (blue) square lattice, pointing inside or outside the vertex. b) The projection breaks the symmetry of the problem. Since the first nearest neighbour (spins perpendicular to each other in the vertex) and the second neighbour (parallel spins) have different distances, they have different coupling strength constants J_1 and J_2, respectively.

If we consider the spin in a square spin system to only interact with their first and second neighbour (in both vertices they are forming), then the system can be described with the vertex models as it often is. The following sections will describe the vertex models [4, 26] based on the square geometry.

4.1. Six vertex model

The six vertex model is a model which considers only the existence of the configurations which follow the ice-rule [27, 28]. Therefore only possible vertex configurations are Type I and Type II, as shown in Figure 4.2. The other types are disregard. However, since the symmetry of the vertex is broken and the coupling constant between the first nearest neighbours J_1 and the second nearest neighbour J_2 are generally not equivalent, there are three different realisations of the six vertex model:

Slater-KDP model where the $J_1 < J_2$, therefore, Type II vertices have lower energy and are ground state configurations and Type I are excitations.

Ice model, where the $J_1 = J_2$ and, therefore, the energies of both Type I and Type II are equal, and both types are ground state configurations.

The third possible realisation of the six vertex model is *Rys-F model*, where $J_1 > J_2$ and Type I vertex configuration is ground state one and Type II vertices are excitations.

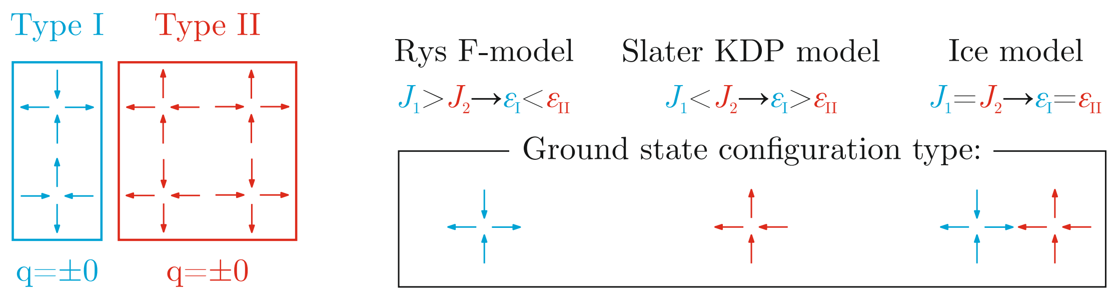

Figure 4.2: The six vertex model. Depending on the relation between the J_1 and J_2 coupling constant there are three realisation of the six vertex model.

Rys F model

In the case that the J_1 coupling strength constant is bigger than J_2, the system is described by the Rys F model. In this model, the energy of the Type I vertices is smaller than the Type II. One of the two possible ground state phases is shown in Figure 4.3 a).

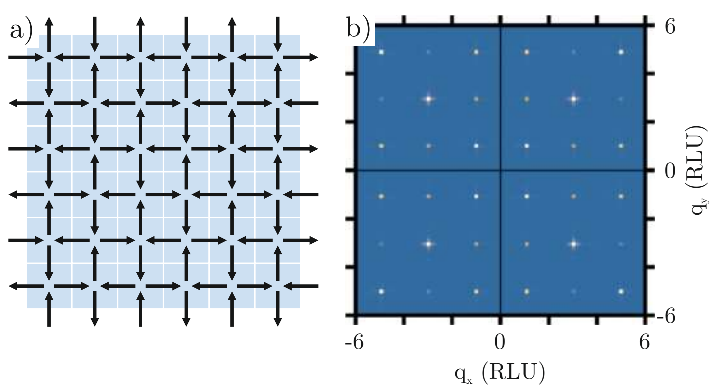

Figure 4.3: a) Example of real space ground state configuration of Rys F model, the Type I vertices are perfectly ordered across the lattice. b) Example of Rys F model MSF, where Bragg peaks indicate complete order. Images were taken and modified from [8].

The ground state phase is two times degenerated and perfectly ordered. Therefore, the MSF associated with this model show high intensive Bragg peaks all over the reciprocal space.

In 1967, Lieb [29] solved the Rys F model and showed that the phase transition from the ground state to the high-energy phase is of infinite order [4] with order parameter which is infinitely smooth [30]. The high-energy phase of the F model is the mixture of the Type I and Type II vertices with the ratio 1:2, the same as in the Slater KDP model.

The specifics of this model will be discussed in more detail in section 4.3, where experimental analysis of the unique phase transition will be provided.

4.2. Tuning the coupling constant

After the pioneering work done by Wang et al. [3], Möller and Moessner [31] introduced theoretical proposition how to renew the degeneracy of Wang's system to reach the Ice model realisation. To do so, the J coupling strength constant needs to be tune so that the ratio between the $J_1/J_2 = 1$. In the following sections there will be presented three different approaches, which successfully regained the degeneracy of the spin ice systems.

4.2.1. Square lattice with hole

In this thesis and [32], we present another way to tune the J coupling constant. Instead of having lattices made by single-domain nanomagnets that interact via dipolar interaction, we employ a similar strategy to the square lattice as we did with the kagome systems. The central idea of our approach is to connect the nanomagnets into one lattice. The system is transformed from a spin system where dipolar-driven many-body interactions are the driving force into one macro-object where the configuration at the vertex site is decided by competing micromagnetic energies. Thus we are effectively fabricating lattices suitable for studying vertex models since the lattice's driving force are micromagnetic forces forming the domain walls at the vertex site, and the vertices only interact with the shared nanomagnet.

An example of our lattice is shown in Figure 4.4 a). Part of the magnetic material has been removed from the vertex site, and only an empty hole remains. This defect plays a crucial role in tuning the energy of the domain walls at the vertex site. The resulting magnetisation configuration associated with each vertex type is shown in Figure 4.4 b). It can be seen that Type I domain wall forms an anti-vortex. Type II configuration resembles a homogeneously polarised domain wall across the vertex. Type III is similar to Néel transverse domain wall, and Type IV is a vortex domain wall.

The effect of the hole defect was theoretically analysed by micromagnetic simulations performed by Mumax3 code. The simulation parameters were set to resemble the real lattices. The spontaneous magnetisation was set $M_\mathrm{S} = 8 \times 10^5$ A/m, the exchange stiffness was set to 10 pJ/m and dumping coefficient $\alpha = 0.5$, hence the dynamics were not taken into account. Magnetocrystalline anisotropy was neglected since the material used in the experiment was permalloy. The simulation mesh size was set to $1 \times 1 \times 25$ nm.

The energy hierarchy of the vertex types can be finely tuned by changing the hole diameter at the vertex site as is shown in Figure 4.4 c), where results of micromagnetic simulations are plotted.

Energies of Type I and Type II vertices evolve opposite trends as the hole diameter increases. Type I magnetisation texture have an out-of-plane core in the centre of the

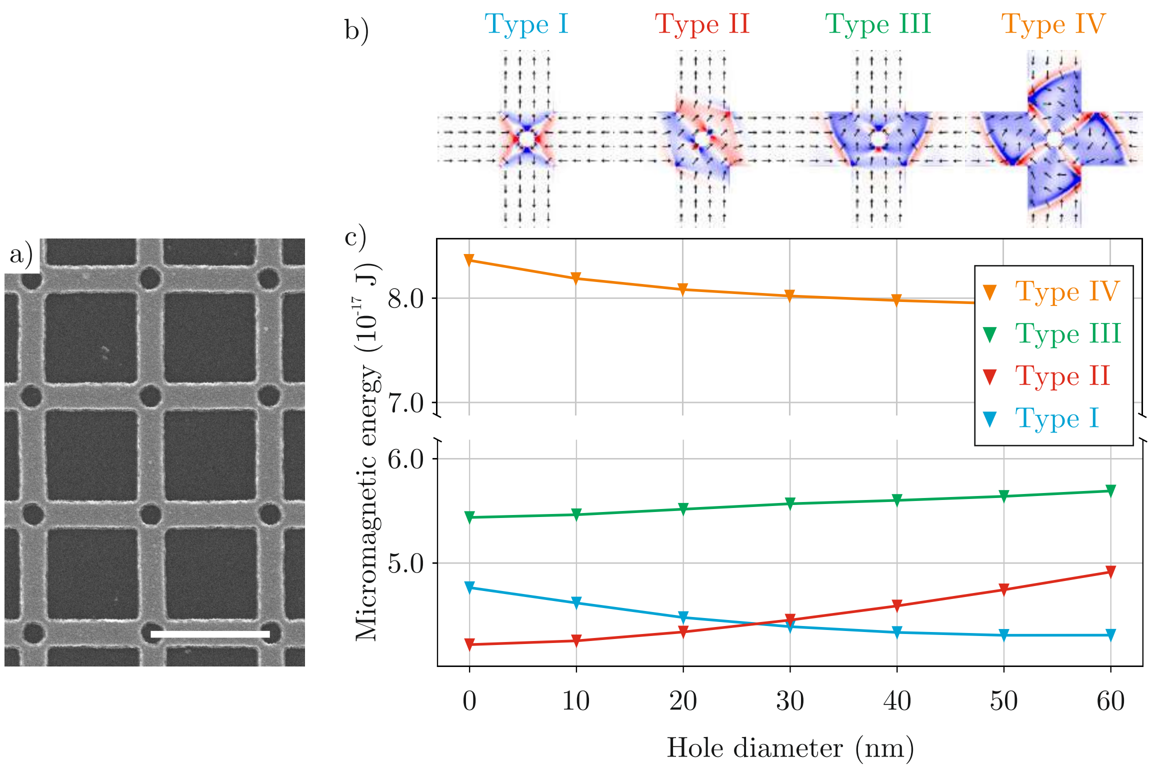

Figure 4.4: a) SEM image of one example of macrolattice with holes, the scale bar is 500 nm. b) Micromagnetic configurations of Type I, II, III and IV vertices. Black arrows show the direction of magnetisation. Blue and red contrast highlight the divergence of the magnetisation vector. c) Total energy of the vertex types depending on the hole diameter. Taken and edited from [32].

domain wall. Therefore if the system has no hole or a small diameter, it costs more energy to stabilise Type I configuration. However, as the hole expands and the magnetic material where the out-of-plane magnetisation should be stabilised is removed, the total energy of the Type I configuration decrease. With the presence of the large hole or entirely disconnected nanomagnets - this lattice prefers Type I vertices everywhere, similar to the Wang realisation as the interaction between first neighbours is stronger than between the second nearest neighbours.

Type II has the lowest energy in a fully connected grid without the hole's presence. As the hole diameter increase, so does the Type II energy. It is caused by an induced curl of the magnetic texture around the hole, which leads to increased exchange energy and the appearance of additional surface magnetic charges at the hole defect, leading to the increasement of demagnetisation energy.

The energies of Type III and Type IV are always[5] higher for the simulated parameters than Type I and II. Type IV was never observed in well-demagnetised lattices, even for large holes. On the other hand, even though the energy of Type III vertices is always higher than Type I or Type II, the energy gap is still small to eliminate the presence of Type III configurations entirely.

[5] If the thickness of the nanomagnets is lowered to approx. 2 nm, the Type III configuration has lower energy than Type I for small holes.

4.3. Experimental realisation of the F model

All the benefits of the square system with holes culminated in the attempt to visualise and analyse the infinite order phase transition of the F model in real space. Inspired by Nisoli's work [33], where the connection between the phase transition of the F model and the topological sectors is investigated, we decided to use Nisoli's description of the system via so-called *Faraday lines* (FL).

The motivation for our work is to investigate the infinitely continuous transition in real space, which was theoretically solved by Lieb [29], Kosterlitz and Thouless [34] and which now can be described by Faraday line representation introduced by Nisoli [33].

As mentioned in section 4.1, the F model has two distinguished properties: Firstly, the system is characterised by infinite order phase transition separating the antiferromagnetic ground state and high-temperature square ice phase. Secondly, the configurational space is divided into topological sectors [32, 33]. Both these properties result from forbidding Type III and IV high-energy vertex configurations. Because of the non-existence of Type III and Type IV vertices and since the system energies of the vertex I and II are $0 = \epsilon_{\mathrm{I}} < \epsilon_{\mathrm{II}}$, the system exhibit only loop excitations made by clusters of Type II vertices.

4.3.1. Faraday lines

The example of the excited configuration of the F model is shown in Figure 4.5 where type II excitations (red background) separate the patches of type I vertices (blue/green) with opposite stagger parameter[6]. Only the type II vertices carry magnetic moments, which can be joined into the Faraday lines.

By definition, in a six-vertex model, FL can only cross vertices diagonally; therefore, every single FL belongs only to one of the sublattices, A or B. The parity of the FL is derived from the sublattice the FL is sitting upon. Throughout this text, the colour code will not change, and FL with A or B parity have a red or blue colour. The FL with different parity cannot cross. Since only the type II vertices have non-zero energy, Faraday lines carry all the system's energy. Therefore they are elementary excitation of the F model [32], and the F model can be described as a loop gas [33].

FL are divided into two very different groups: Chiral closed loops (red FL in Figure 4.5). These types of loops are magnetisation-free. The inside of the closed loop has a vertices configuration with a total magnetisation of zero. Therefore the total magnetisation of the closed loop is always zero as well. This is true even for configurations where there are closed loops within the closed loops. Closed loops can be contracted to zero and do not interact with an external magnetic field since they do not contain any net magnetisation.

The second type of FL are system-spanning windings which carry all the net magnetisation. These FL cannot be contracted, forcing the system to fluctuate within a given topological sector [33, 35]. Examples of such FL are both blue FL shown in Figure 4.5.

[6] Green and blue patches of the type I vertices are shifted by one vertex, hence incompatible and creating Type II vertex configuration.

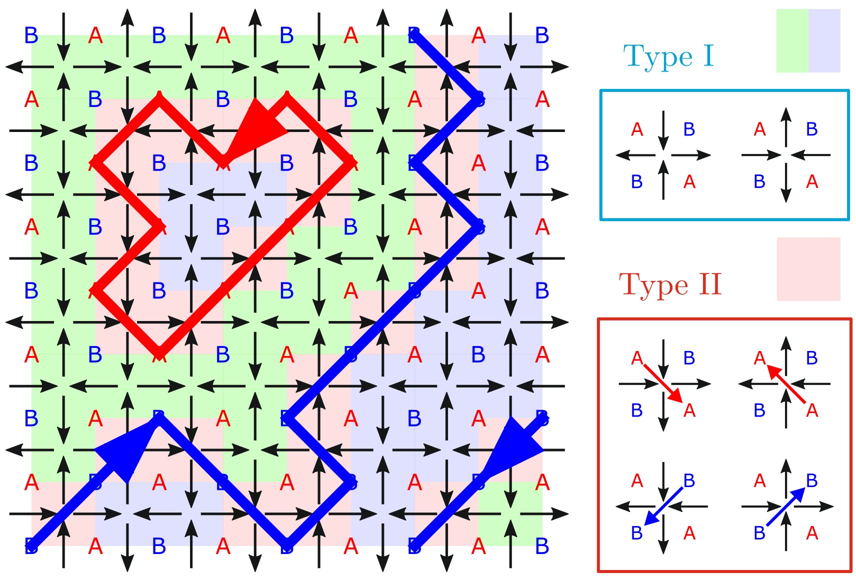

Figure 4.5: An example of an excited configuration of the F model. The type I vertices are depicted with a blue and green background, and the type II vertices are highlighted with red. The lattice can be divided into two alternating sublattices, A and B, as indicated by coloured letters A and B. Type I vertices are fully demagnetised. On the other hand, type II vertices carry magnetic moment, as indicated by the diagonal arrows. The arrow's colour is determined by parity depending on the sublattice they belong to (A is red, B is blue). Taken and edited from [32].

So far, the attempts to probe the topological properties of the F model and its phase transition via two-dimensional lattices of interacting nanomagnets have failed. Even though the Wang lattice and other square geometries have the same ground state as the F model, their thermodynamics is described by the sixteen vertex model since the high-energy vertices (violating the ice-rule constraints) are present at a high rate. Types III and Type IV vertices are sources/sinks of magnetic flux, thus breaking the F model's properties.

In our work, we present how the F model can be approached. With our lattices with holes, we can probe and control the topological properties of the F model as the systems undergo the phase transition from the low-energy antiferromagnetic ground state into the high-energy ice-like phase. All this is possible because the number of Type III defects (which were not entirely suppressed) have marginal contribution since their vertex population is always less than 1 %.

4.3.2. The experimental results

Our prediction has been tested on the series of square lattices with holes. The parameters of fabricated lattices are as follows: the nanomagnets' width is 100 nm, their thickness is 25 nm, and the vertex-to-vertex distance is 500 nm. The hole diameter changes from 70 to 120 nm. Each lattice contains 900 vertices. The material used for the fabrication of such lattices was permalloy. The demagnetisation protocol used to bring the lattices into their ground state configuration was 120 hours long.

For better statistics, several series of lattices were fabricated, all the fabrication parameters were the same for each series and all were exposed to the same demagnetisation protocol.

The measurements were done on lattices with hole diameter $\phi = (120;\ 95;\ 90;\ 85;\ 80;$ and $72)$ nm. The reason for the gap between 120 nm and 95 nm hole diameter is that the changes on the lattices were small in this hole diameter region and the hole diameter 120 nm is the largest one which still does not disconnect the pseudo-spins forming the lattices.

The example of the one series measurement visualised by FL interpretation is shown in Figure 4.6 a) together with the average MSF calculated from all series b).

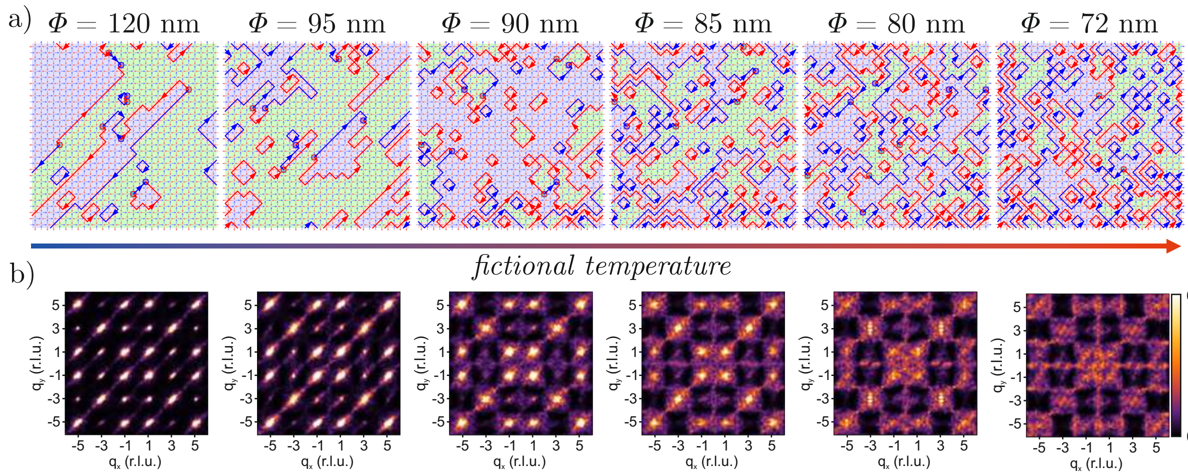

Figure 4.6: a) Real space FL visualisation and b) reciprocal space MSF analysis of the measured series of the lattices with different hole diameters. In the FL visualisation, we observe how two times degenerated antiferromagnetic background (blue and green) is made purely by Type I vertices, which are separated by FL made out of Type II vertices. The FL are blue or red depending on their parity, and their direction is visualised by a small arrow sitting on FL. Red and blue FL never connect, only if the Type III ice-rule-breaking vertex is present, as highlighted by the blue and red circles. Each MSF is averaged over four real space configurations with the same hole diameter (i.e., 3600 vertices) to get a better statistic. MSF covers ± 6 reciprocal lattice units (RLUs), and all are scaled to the same intensity to visualise the evolution better. Taken and edited from [32].

The lattices with large holes are close to the antiferromagnetic ground state, and only a marginal percentage of vertices are other types than Type I. FL separates the two possible ground states with opposite stagger parameters of Type I. As the hole diameter decreases, so do the patches of the ground state and more system excitation (FL made by Type II vertices) starts to emerge. For the lattice with hole diameter 72 nm, the ratio between the populations of Type I and Type II vertices is almost $1:2$ as the population of Type I is 35 % and Type II is almost 65 %. This population is comparable to what is expected from the square ice manifold. Since the change in the hole diameter is small and almost continuous, we can safely assume we are observing the snapshots of the phase transition between the F model antiferromagnetic ground state and its high-energy square ice phase.

As predicted by the simulations, the changes in the hole diameter lead to changes in the magnetic correlations. From the view of the energy gap between the Type I and Type II vertices, it can be said that the holes at the vertex site can be viewed as a heating knob. With the proper adjustments of the hole diameter, the system can be tuned into the Coulomb spin liquid phase [24, 36–38].

To support the claims about observing the phase transition, we compute MSF associated with all lattices. To improve the statistics, each MSF showed in Figure 4.6 b) were averaged over four different lattices (with the same parameters and exposed to the same demagnetisation protocol). Figure 4.6 b) also reveal gradual changes in the spin-spin correlation across the lattices. First, at the low temperature (large hole diameter $\phi \geq 95\,\mathrm{nm}$), we observe intense Bragg peaks in the MSF as the system is, for the most part, perfectly ordered. When the $80 \leq \phi \leq 95\,\mathrm{nm}$, there is visible coexistence of Brag peaks associated with the ordering and ice-like disordered background. This background dominates as the Bragg peaks faint when heating the system. For the $\phi = 72\,\mathrm{nm}$, the MSF shows a pattern associated with the square ice regime, i.e. diffused but structured [24, 36].

We want to emphasise that the magnetic correlations are affected even by the smallest step in the hole diameter (possible by the lithograph technique). The results we obtain are consistent over all the 24 lattices, proving the results are robust and series independent. We consistently start with large patches of antiferromagnetically ordered background for lattices with large hole diameters. We can reach the low-energy regime for lattices with $\phi = 72\,\mathrm{nm}$.

To proclaim that we are working within the framework of the six-vertex model would be incorrect. The crucial benefit of our approach, resulting from the fact that the nanomagnets are connected, is the low percentage of Type III defects. Even with a long demagnetisation protocol, we still observe a non-zero population of the Type III vertices. These ice-rule-breaking configurations are always highlighted by a coloured circle and connect two FL with opposite parity. However, as mentioned before, the percentage of Type III vertices is typically 1 % or less, which is almost ten times less than in previous works with height offsets [24, 36], where field-driven demagnetisation was used.

The presence of Type III destroys the physics of the F model, however since we have such a small portion of the Type III defects, especially compared to the number of FL, we observe[7] we believe that our systems can be a good approximation of the F model.

Since our motivation is to describe the phase evolution of the F model and we believe that we are in good approximation to that model, we decided to use Nisoli's approach and analyse the FL. The FL we measured experimentally can be divided into two parts: Closed, chiral loops and open FL, where chirality is not defined. Open FL should not theoretically exist. However, since our systems have finite sites and non-periodic boundaries, the open FL span across the system and are anchored to the boundaries. Open FL carry the net polarisation. Both of these types of FL have defined parity. Chirality and parity are good indicators that our systems or demagnetisation protocol do not suffer from inherent bias.

The complex analysis of FL is shown in Figure 4.7. It is shown in the histogram in Figure 4.7 a) that both possible types of parity and chirality are equally populated in our experiment. Two main features were observed in the FL visualisation. The loop density is one of them. There is a visible increase in the loop density when the hole diameter decrease. This effect is evident for the smallest possible loops, in which the population increase in the order of magnitude through the series measurement as shown in Figure 4.7 b). This observation is direct evidence of the contraction of the FL as the system approaches its antiferromagnetic ground state [32].

[7] There is typically ten times more FL than the Type III vertices when $\phi < 85\,\mathrm{nm}$ [32].

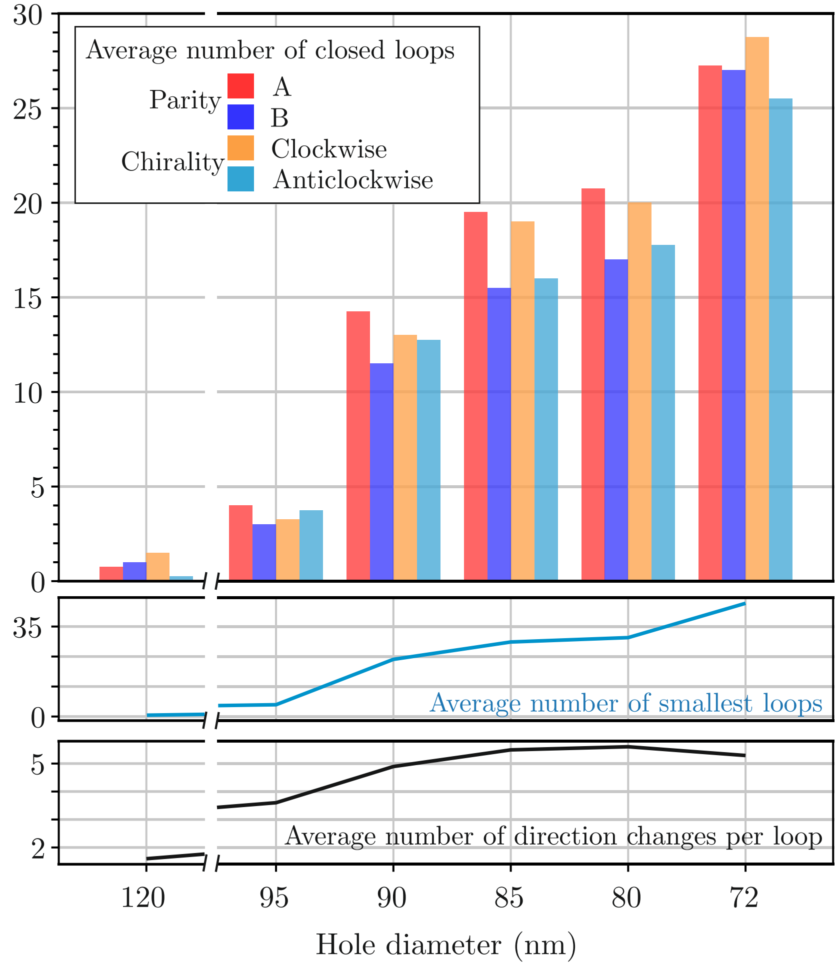

Figure 4.7: Analysis of the FL properties averaged from four lattices for each hole diameter. The Faraday loops are characterised by parity (A or B) and chirality (clockwise or anticlockwise). a) The histogram shows that both quantities are equally populated. Hence the experiment does not suffer from inherent or demagnetisation bias. b) An average number of the smallest possible Faraday loops, and c) an average number of changes in the direction of Faraday loops. Taken and edited from [32].

The changes in the FL curvature were the second interesting feature observed due to the real space measurement. We plot average numbers of direction changes in Figure 4.7 c). When the system is approaching the ice regime FL have a meandering shape. On the other hand, when the antiferromagnetic patches are large, the FL are straight. This behaviour is probably a consequence of the tension of the antiferromagnetic background domains.

Chapter 5: Concluding remarks

The presented work gives a brief overview of the origin of artificial systems and frustrated materials. A description of the peculiar behaviour of frozen water and its puzzling properties is provided, as well as its similarity to the magnetically frustrated spin ice systems. Artificial spin ice systems are specially designed to mimic the behaviour of real natural materials but as two-dimension systems, which can serve as an almost unlimited playground for researching the statistical models and exotic physics of spin liquids and magnetic monopoles.

We focused our research on two types of artificial spin systems: kagome and square dipolar spin systems. Both systems are designed to allow us to directly measure the individual spin degree of freedom in a real space with imaging techniques such as MFM.

The main problem of the kagome dipolar spin system that we addressed in this work was the inability of the system to undergo the phase transition into its low-energy manifold. This problem is caused by the dynamical freezing [13], and we were able to bypass it by imprinting the desired phase into the topography of the lattice. Even though we destroyed the system's symmetry, we could still prove that our modified systems were not stuck at one effective temperature and could be heated up and shifted in the thermodynamic profile. We still observe both correlation coefficients and MSF, which perfectly correspond with the theoretical prediction for the kagome dipolar spin ice system. We were able to design lattices, where only by use of the field-driven demagnetisation protocol, the spins were self-ordered into configurations belonging to the long range order and spin liquid 2 phase. The ability to imprint any t hinkable spin configuration comes at the cost of changing the system's Hamiltonian and related thermodynamic profile. The unanswered question concerning the kagome lattice with notches is, how is it possible to observe a perfect fit with the thermodynamics of kagome dipolar spin ice when the Hamiltonians are different?

While we did break the symmetry of the kagome dipolar system when using the notches to imprint desired phases, it was the other way around with the square system. The square dipolar spin system lost its symmetry during the transformation process from the three-dimensional crystals. By connecting the system and tuning the energies of the vertices, we regained the lost degeneracy and restored the system symmetry. We managed to tune the system to capture the physics of Coulomb spin liquid. The vital advantage of our square system with hole is a low number of high-energy vertices configurations. Therefore, it can be used to emulate the behaviour of the celebrated six-vertex model. By carefully tuning the hole's diameter and starting from the proper configuration, we provided the first attempt to visualise the phase transition of the F model in real space. Not only were we successful in proving the theoretical concepts of the Faraday lines defined by Nisoli [33] (as much as the finite size systems allowed us), we also provided new observations about the model behaviour during the phase transition that were not deduced theoretically such as a role of the background tension on the properties of the Faraday lines.

Due to its properties, the square lattice with a hole is suitable for further research of the F model, where are still plenty of questions unanswered, such as the role of the monopole dynamics in the ice regime, a fluctuation between the topological sectors, response to the external magnetic field and so on.

The reason we were able to address these scientific problems successfully is our innovative strategy. Instead of fabricating the systems where the dipolar interactions between all elements try to minimise the system energy, with our design, we switched from the spin systems to the vertex systems. The simplicity of this approach allowed us to bypass the many-body interaction and focus solely on the tuning of the micromagnetic energies forming domain walls at the vertex sites. We even discovered that from the point of view of the energy gap between the ground state configuration and system excitation, both topological defects (notch and hole) could serve as a system heater. We tied the external geometrical parameter with the internal temperature of the system. All this while working at room temperature with athermal systems.

We want to emphasise that this approach is not restricted to use only on kagome or square lattice. Almost any currently studied lattices with in-plane magnetisation [39, 40] can be modified similarly to our systems.

If the lattice is connected and the system has asymmetrical vertices, using the notches with the right parameters can be helpful in tuning the favourable spin configurations without any additional symmetry breaking. The lattices which could be easily modified with the notch are, for example Santa Fe, Tetris, Brickwall or Shakti lattices.

When there is a need for recovering or retaining the symmetry in the systems with symmetrical vertices, one might consider using hole (or even square) defects to tune the energy of the incurred vertex configuration, for example, in Square, Toroidal, kagome, Voretex, Pentagonal and Dice lattices.

In all the lattices mentioned above, the easy way to imprint desirable configurations can be used to study the interface of individual phases.

Reference list

[1] M. Tanaka *et al.*, "Domain structures and magnetic ice-order in nife nano-network with honeycomb structure," *Journal of applied physics*, vol. 97, no. 10, p. 10J710, 2005.

[2] M. Tanaka *et al.*, "Magnetic interactions in a ferromagnetic honeycomb nanoscale network," *Physical Review B*, vol. 73, no. 5, p. 052411, 2006.

[3] R. F. Wang *et al.*, "Artificial spin ice in a geometrically frustrated lattice of nanoscale ferromagnetic islands," *Nature*, vol. 439, 2006.

[4] E. H. Lieb, *Exact Solution of the F Model of an Antiferroelectric*, pp. 453–455. Berlin, Heidelberg: Springer Berlin Heidelberg, 2004.

[5] A. Broers, "Resolution limits for electron-beam lithography," *IBM Journal of Research and Development*, vol. 32, no. 4, pp. 502–513, 1988.

[6] W. Hu *et al.*, "Sub-10 nm electron beam lithography using cold development of poly (methylmethacrylate)," *Journal of Vacuum Science & Technology B: Microelectronics and Nanometer Structures Processing, Measurement, and Phenomena*, vol. 22, no. 4, pp. 1711–1716, 2004.

[7] Y. Perrin, *Réseaux artificiels à frustration géométrique.* PhD thesis, Université Grenoble Alpes, 2016.

[8] N. Rougemaille and B. Canals, "Cooperative magnetic phenomena in artificial spin systems: spin liquids, coulomb phase and fragmentation of magnetism," *The European Physical Journal B*, vol. 92, 2019.

[9] Y. Qi, T. Brintlinger, and J. Cumings, "Direct observation of the ice rule in an artificial kagome spin ice," *Physical Review B*, vol. 77, no. 9, p. 094418, 2008.

[10] I. A. Chioar *et al.*, "Nonuniversality of artificial frustrated spin systems," *Physical Review B*, vol. 90, no. 6, p. 064411, 2014.

[11] J. Colbois *et al.*, "Artificial out-of-plane ising antiferromagnet on the kagome lattice with very small farther-neighbor couplings," *Physical Review B*, vol. 104, no. 2, p. 024418, 2021.

[12] B. Canals *et al.*, "Fragmentation of magnetism in artificial kagome dipolar spin ice," *Nature communications*, vol. 7, no. 1, pp. 1–6, 2016.

[13] V. Schánilec *et al.*, "Bypassing dynamical freezing in artificial kagome ice," *Physical Review Letters*, vol. 125, 2020.

[14] G. Möller and R. Moessner, "Magnetic multipole analysis of kagome and artificial spin-ice dipolar arrays," *Physical Review B*, vol. 80, no. 14, p. 140409, 2009.

[15] G.-W. Chern, P. Mellado, and O. Tchernyshyov, "Two-stage ordering of spins in dipolar spin ice on the kagome lattice," *Phys. Rev. Lett.*, vol. 106, p. 207202, 2011.

[16] N. Rougemaille *et al.*, "Artificial kagome arrays of nanomagnets: a frozen dipolar spin ice," *Physical Review Letters*, vol. 106, no. 5, p. 057209, 2011.

[17] L. Anghinolfi, H. Luetkens, J. Perron, M. Flokstra, O. Sendetskyi, A. Suter, T. Prokscha, P. Derlet, S. Lee, and L. Heyderman, "Thermodynamic phase transitions in a frustrated magnetic metamaterial," *Nature communications*, vol. 6, no. 1, pp. 1–6, 2015.

[18] J. C. Gartside *et al.*, "Realization of ground state in artificial kagome spin ice via topological defect-driven magnetic writing," *Nature Nanotechnology*, vol. 13, 2018.

[19] N. Rougemaille *et al.*, "Chiral nature of magnetic monopoles in artificial spin ice," *New Journal of Physics*, vol. 15, no. 3, p. 035026, 2013.

[20] S. Gliga *et al.*, "Spectral analysis of topological defects in an artificial spin-ice lattice," *Physical review letters*, vol. 110, no. 11, p. 117205, 2013.

[21] V. Nguyen *et al.*, "Competing interactions in artificial spin chains," *Physical Review B*, vol. 96, no. 1, p. 014402, 2017.

[22] Y. Perrin, B. Canals, and N. Rougemaille, "Quasidegenerate ice manifold in a purely two-dimensional square array of nanomagnets," *Physical Review B*, vol. 99, no. 22, p. 224434, 2019.

[23] A. Vansteenkiste *et al.*, "The design and verification of MuMax^3," *American Institute of Physics*, vol. 4, 2014.

[24] Y. Perrin, B. Canals, and N. Rougemaille, "Extensive degeneracy, Coulomb phase and magnetic monopoles in artificial square ice," *Nature*, vol. 540, 2016.

[25] S. Kempinger *et al.*, "Imaging the stochastic microstructure and dynamic development of correlations in perpendicular artificial spin ice," *Physical Review Research*, vol. 2, no. 1, p. 012001, 2020.

[26] R. J. Baxter, *Exactly solved models in statistical mechanics.* Elsevier, 2016.

[27] L. Pauling, "The structure and entropy of ice and of other crystals with some randomness of atomic arrangement," *Journal of the American Chemical Society*, vol. 57, no. 12, pp. 2680–2684, 1935.

[28] J. D. Bernal and R. Fowler, "A theory of water and ionic solution, with particular reference to hydrogen and hydroxyl ions," *The Journal of Chemical Physics*, vol. 1, 1933.

[29] E. H. Lieb, "Exact solution of the problem of the entropy of two-dimensional ice," *Physical Review Letters*, vol. 18, no. 17, p. 692, 1967.

[30] R. Baxter, "Spontaneous staggered polarization of thef-model," *Journal of Statistical Physics*, vol. 9, no. 2, pp. 145–182, 1973.

[31] R. Möller, G. Moessner, "Artificial square ice and related dipolar nanoarrays," *Physical Review Letters*, vol. 96, 2006.

[32] V. Schánilec *et al.*, “Approaching the topological low-energy physics of the f model in a two-dimensional magnetic lattice,” *Physical Review Letters*, vol. 129, no. 2, p. 027202, 2022.

[33] C. Nisoli, “Equilibrium field theory of magnetic monopoles in degenerate square spin ice: Correlations, entropic interactions, and charge screening regimes,” *Physical Review B*, vol. 102, no. 22, p. 220401, 2020.

[34] J. M. Kosterlitz and D. J. Thouless, “Ordering, metastability and phase transitions in two-dimensional systems,” *Journal of Physics C: Solid State Physics*, vol. 6, no. 7, p. 1181, 1973.

[35] D. M. Arroo and S. T. Bramwell, “Experimental measures of topological sector fluctuations in the f-model,” *Physical Review B*, vol. 102, no. 21, p. 214427, 2020.

[36] O. Brunn, Y. Perrin, B. Canals, and N. Rougemaille, “Signatures of farther neighbor couplings in artificial square ice,” *Physical Review B*, vol. 103, no. 9, p. 094405, 2021.

[37] A. Farhan *et al.*, “Emergent magnetic monopole dynamics in macroscopically degenerate artificial spin ice,” *Science advances*, vol. 5, no. 2, p. 6380, 2019.

[38] E. Östman *et al.*, “Interaction modifiers in artificial spin ices,” *Nature Physics*, vol. 14, no. 4, pp. 375–379, 2018.

[39] S. H. Skjærvø, , *et al.*, “Advances in artificial spin ice,” *Nature Reviews Physics*, vol. 2, no. 1, pp. 13–28, 2020.

[40] X. Zhang *et al.*, “Emergent strings in santa fe artificial spin ice,” in *APS March Meeting Abstracts*, vol. 2021, pp. C39–003, 2021.